Contents

Appendix A. Summary of Facilities

Table A.1: Facility ID, operational capacity, and average inmate population (throughout study period).

Facility	Occupational Capacity	Population Summary		
		Min	Max	Weekly Average
A	300	119	265	170·09
B	320	195	301	227·47
C	1930	1374	1800	1604·34
D	982	389	804	485·61
E	733	485	673	552·17
F	914	402	776	484·10
G	1055	653	843	765·22
H	866	665	822	754·18
I	1062	789	976	890·93
J	1204	973	1068	1022·72
K	1270	989	1225	1138·09
L	1238	681	1119	952·90
M	621	193	572	409·07
N	730	392	693	497·96

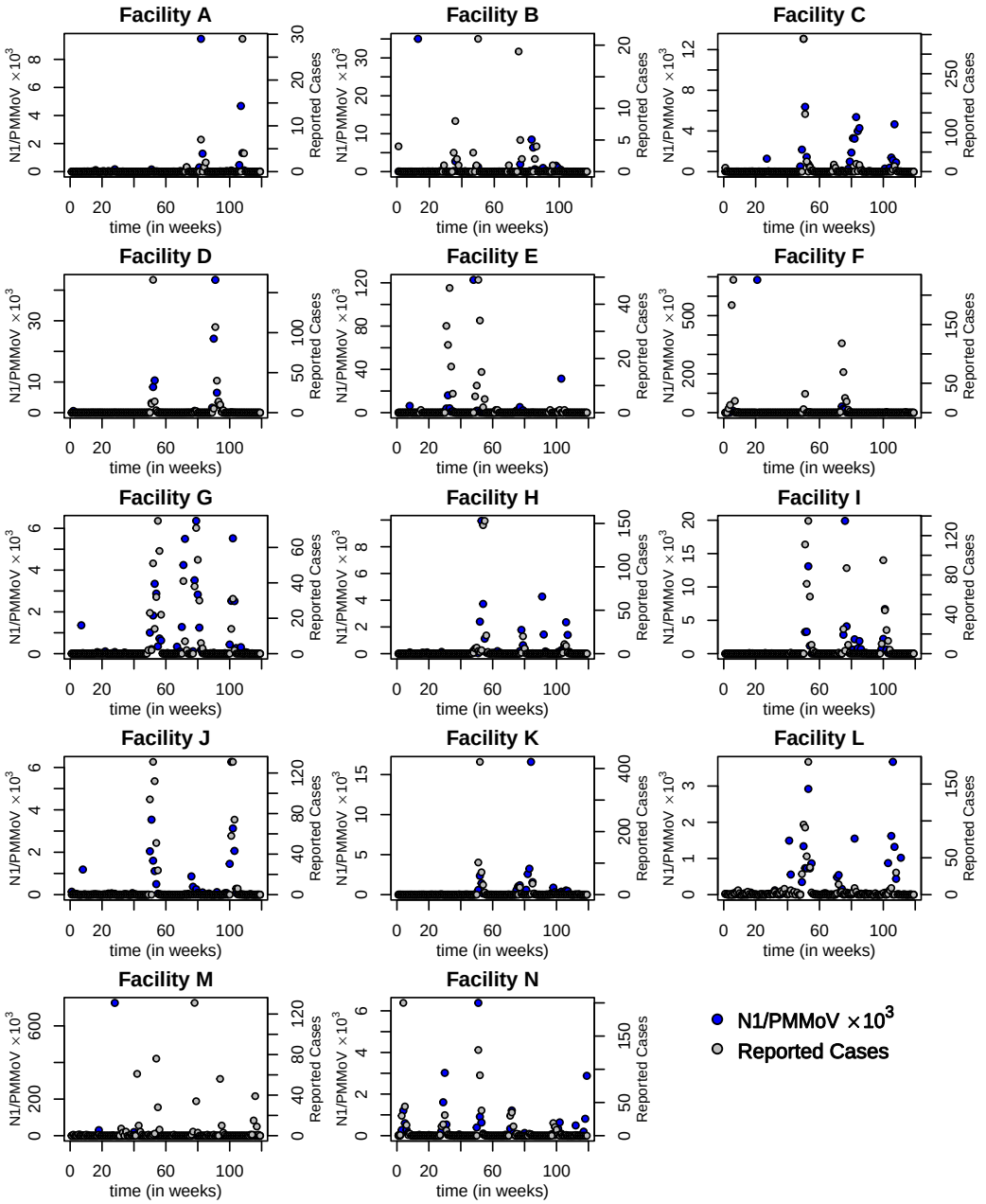

Figure A.1: The SARS-CoV-2 (N1) copies per ml normalized by pepper mild mottle virus (PMMoV) copies per ml as a ratio for each facility (right y-axis) throughout time compared to the observed number of inmate positive COVID-19 cases (left y-axis).

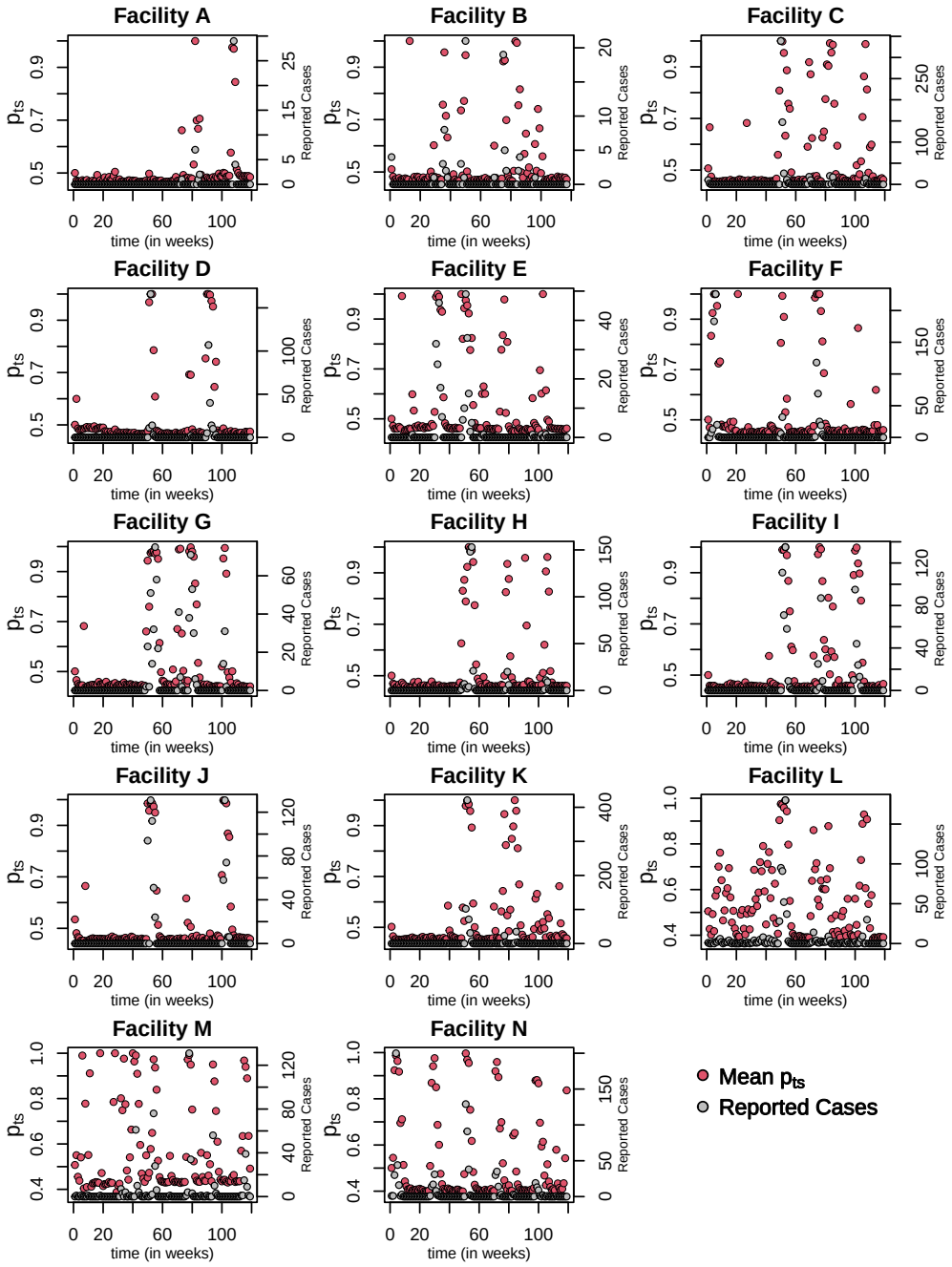

Figure A.2: Estimated p_{ts} probabilities, the probability of at least one positive case versus the number of reported cases, Z_{ts}, by facility.

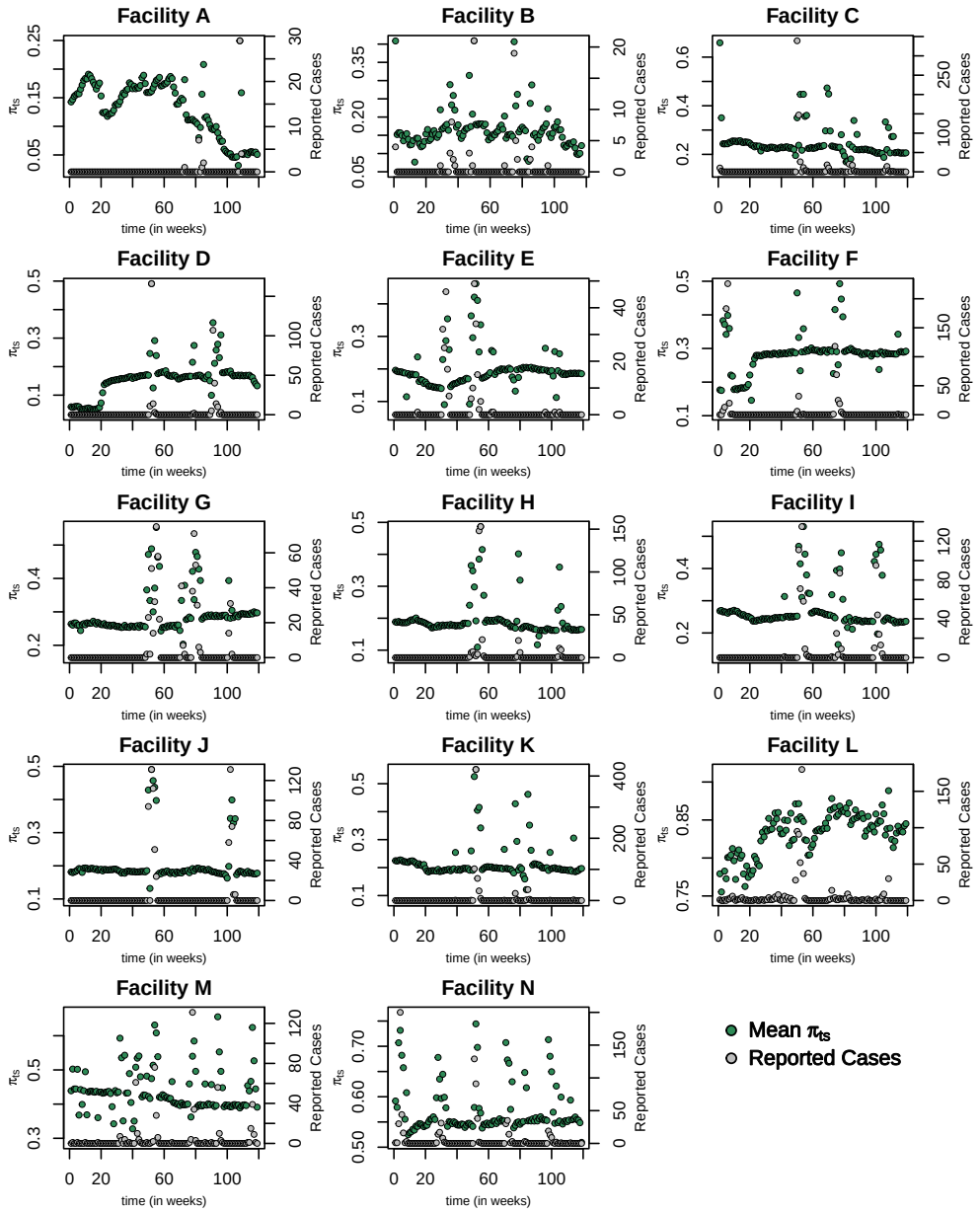

Figure A.3: Estimated reporting probabilities π_{ts} for each facility s compared to the reported number of positive inmate COVID-19 cases.

Appendix B. Hierarchical Spatial-temporal Model with Lags for Underreporting Data

Let N_{ts} and Z_{ts} denote, respectively, the true but unobserved number of positive COVID-19 cases and the recorded (observed) number of cases for location $s \in \{1, 2, \cdots, J\}$ at time t, $t = 1, 2, 3, \cdots, N$. Assume each location s, $s \in \{1, 2, 3, \cdots, J\}$ has different independent reporting probabilities π_{ts} at time t due to the distinct situations present in different correctional facilities such as sampling methods and testing capabilities. Then conditional on the true positive cases number N_{ts}, the time series of counts Z_{ts} reported at time t at location s follows a Binomial distribution with probability π_{ts}:

$$Z_{ts}|N_{ts} \sim Binomial\left(N_{ts}, \pi_{ts}\right) \tag{B.1}$$

We will assume that the reporting probabilities π_{ts} in (B.1) depend on a set of covariates such as inmate population and capacity ratio. Denote the design matrix containing these covariates by $X_{ts}^{(1)}$ and the reporting probability π_{ts} is modeled by a logistic regression on X_{ts}^{1}:

$$\log\left(\frac{\pi_{ts}}{1-\pi_{ts}}\right) = X_{ts}^{(1)}\vec{\beta_s} + \varepsilon_{ts} = \psi_{ts} \tag{B.2}$$

where $\vec{\beta_s}$ is the $N \times 1$ vector of the regression coefficients, $\vec{\beta_s}$ has normal prior with mean m_{β_0} and covariance matrix P_{β_0}. The white noise error term ε_{ts} has the normal prior with mean $\mu_{\varepsilon_{0,s}}$ and variance $\sigma^2_{\varepsilon_{0,s}}$.

Assume the number of true positive COVID-19 cases N_{ts} at location s at time t follows a latent Poisson distribution with rate λ_{ts}, which is a Gamma distribution with shape parameter $h = 1$ and scale parameter $\dfrac{p_{ts}}{1-p_{ts}}$.

$$N_{ts}|\lambda_{ts} \sim Poisson\left(\lambda_{ts}\right) \tag{B.3}$$

$$\lambda_{ts}|p_{ts} \sim \mathcal{G}amma\left(h, \frac{p_{ts}}{1-p_{ts}}\right) \tag{B.4}$$

If we marginalize over λ_{ts}, we get a negative binomial marginal distribution for N_{ts}:

$$P(N_{ts} = k \,|\, h, p_{ts}) = \frac{\Gamma(k+h)}{k!\Gamma(h)}(1-p_{ts})^h p_{ts}^{N_{ts}} \tag{B.5}$$

Thus p_{ts} is the probability of at least one positive case at t in the facility s, i.e, $p_{ts} = P(N_{ts} \geq 1)$. To capture the hidden dynamic lagged effects, p_{ts} is modeled as a logistic regression embedded with an auto-regressive latent process γ_{ts} with order 1 (AR(1) process). The MCMC algorithm for the more generalized higher-order AR(p) can be extended easily based on the current model.

$$\log\left(\frac{p_{ts}}{1-p_{ts}}\right) = X_{ts}^{(2)} + \gamma_{ts} = \phi_{ts} \tag{B.6}$$

$$\gamma_{ts} = a_s \gamma_{t-1,s} + e_{ts} \tag{B.7}$$

where $X_{ts}^{(2)}$ is a matrix of relevant factors related to true positive cases. In this paper, we use the normalized SARS-CoV-2 (N1) copies per ml normalized by pepper mild mottle virus (PMMoV) copies per ml as a ratio as $X_{ts}^{(2)}$. And the error term e_{ts} follows normal distribution with mean 0 and variance $\sigma_{e_{0,s}}^2$. The parameter a_s has truncated normal distribution on $(-1, 1)$ as the prior, that is $a_s \sim Normal\left(\mu_{a_{0,s}}, \sigma_{a_{0,s}}^2\right)\mathcal{I}(-1 < a_s < 1)$.

In the realm of spatial-temporal models with lagged effects, it is observed that the majority of models do not take into account the underreporting situation from the systematic review of COVID-19 models[1] and recent various publications.[2–6] This highlights a critical gap in the existing literature. Moreover, current underreport count time series models, such as the widely used Poisson-Logistic (Pogit) model,[7] do not incorporate lagged effects. This limitation restricts their ability to capture the temporal dynamics and delays in reporting COVID-19 cases accurately.

In addition, existing hierarchical count models for the under-reporting type data often rely on benchmarks like mortality rates[8] or overall population numbers from census data[9] to infer the true number of positive cases. However, when studying the relationship between positive COVID-19 cases and wastewater virus concentration, the dynamic movement of the population presents a significant challenge. The movement of individuals within a community, encompassing their residences, workplaces, and public spaces, introduces complexities in accurately tracking the corresponding population numbers within specific sewer sheds. This dynamic nature of population movement makes it difficult to establish a direct and precise correlation between the number of positive cases and the virus concentration in wastewater samples from specific sewer sheds.

In the context of studying prison cases, these issues can be circumvented. The controlled environment of correctional facilities allows for more accurate tracking of the population and their movement, minimizing the challenges associated with population dynamics. By focusing on corrections facility cases, the study can provide valuable insights into the relationship between positive COVID-19 cases and wastewater virus concentration, avoiding the complexities arising from population movement in the broader community.

Appendix C. MCMC sampling

If we marginalize over λ_{ts}, we obtain a negative binomial distribution for N_{ts},

$$p\left(N_{ts}|h,p_{ts}\right) \propto \left(1-p_{ts}\right)^{h}\, p_{ts}^{N_{ts}}\ , \tag{C.1}$$

ignoring constant of proportionality, i.e., $N_{ts}|h,p_{ts} \sim \text{NegBin}\left(h,p_{ts}\right)$. Using a logit transform, we obtain

$$p_{ts}=\frac{e^{\phi_{ts}}}{1+e^{\phi_{ts}}} \Rightarrow \quad p\left(N_{ts}|h,p_{ts}\right) \propto \frac{\left(e^{\phi_{ts}}\right)^{N_{ts}}}{\left(1+e^{\phi_{ts}}\right)^{h+N_{ts}}} \tag{C.2}$$

In this study, we employ a Pólya-Gamma data-augmentation strategy to facilitate the fast fully Bayesian inference using Gibbs sampling. We make use of the following theorem studied by Nicholas Polson and his coauthors:[10]

Theorem 1. *Let $p(\omega)$ denote the density of the random variable $\omega \sim \mathcal{PG}(b,0)$ for $b>0$, where $\mathcal{PG}(\cdot,\cdot)$ denotes the Polya-Gamma distribution. Then, the following integral identity holds for all $a \in \mathbb{R}$,*

$$\frac{\left(e^{\psi}\right)^{a}}{\left(1+e^{\psi}\right)^{b}} = 2^{-b}e^{\kappa\psi}\int_{0}^{\infty} e^{\omega\,\psi^{2}/2}p(\omega)d\omega \tag{C.3}$$

where $\kappa = a-b/2$. Moreover, treating the integrand in (C.3) as an unnormalized joint density $(\psi|\omega)$ gives rise to the conditional distribution

$$p(\omega|\psi) = \frac{e^{-\omega\psi^{2}/2}\,p(\omega)}{\int_{0}^{\infty} e^{-\omega\psi^{2}/2}\,p(\omega)\,d\omega}\ , \tag{C.4}$$

which is also in the Polya-Gamma class: $(\omega|\psi) \sim \mathcal{PG}\left(b,\psi\right)$.

Sampling of a_s:

Let $\vec{\gamma_s} = [\gamma_{t-1,s}]_{t=1}^n$. We find the conditional posterior distribution of a_s,

$$p\left(a_s \,|\, \cdot\right) \propto \prod_{t=1}^{n} p\left(N_{ts} \,|\, \phi_{ts}\right) p\left(\phi_{ts} \,|\, a_s, \sigma^2_{e_{0,s}}\right) p(a_s) \tag{C.5}$$

$$\propto \prod_{t=1}^{n} \frac{\left(e^{\phi_{ts}}\right)^{N_{ts}}}{\left(1+e^{\phi_{ts}}\right)^{h+N_{ts}}} \frac{e^{\frac{1}{2\sigma^2_{e_{0,s}}}(\phi_{ts}-X^{(2)}_{ts}-a_s\vec{\gamma_s})^2}}{\sqrt{2\pi\sigma^2_{e_{0,s}}}} \frac{e^{\frac{1}{2\sigma^2_{a_{0,s}}}(a_s-\mu_{a_{0,s}})^2}}{\sqrt{2\pi\sigma^2_{a_{0,s}}}} \tag{C.6}$$

Using the integral identity (C.3), we can re-write the above in terms of ϕ_{ts},

$$p\left(a_s \,|\, \cdot\right) \propto \prod_{t=1}^{n} 2^{-N_{ts}-h} e^{\kappa^{(2)}_{ts}\phi_{ts}} \int_0^\infty e^{\omega^{(2)}_{ts}\phi^2_{ts}/2}\, p\left(\omega^{(2)}\right) d\omega^{(2)}$$
$$\cdot \frac{e^{\frac{1}{2\sigma^2_{e_{0,s}}}(\phi_{ts}-X^2_{ts}-a_s\vec{\gamma_s})^2}}{\sqrt{2\pi\sigma^2_{e_{0,s}}}} \frac{e^{\frac{1}{2\sigma^2_{a_{0,s}}}(a_s-\mu_{a_{0,s}})^2}}{\sqrt{2\pi\sigma^2_{a_{0,s}}}} \tag{C.7}$$

where $\kappa^{(2)}_{ts} = N_{ts} - \frac{h+N_{ts}}{2} = \frac{N_{ts}-h}{2}$. It follows from Theorem 1 that the mixing distribution is $\omega^{(2)}_{ts}|\phi_{ts} \sim \mathcal{PG}\left(N_{ts}+h, \phi_{ts}\right)$. Let $\vec{\kappa_s}^{(2)} = \left(\left[\kappa^{(2)}_{ts}\right]_{t=1}^n\right)^T$, $Z^{(2)}_s = \left(\left[\frac{ks^{(2)}}{\omega^{(2)}_{ts}}\right]_{t=1}^n\right)^T$ and $\Omega^{(2)}_s = \text{diag}\left(\omega^{(2)}_{1s}, \cdots, \omega^{(2)}_{ns}\right)$. Then,

$$p\left(a_s \,|\, \cdot\right) \propto \int_0^\infty \prod_{t=1}^{n} e^{-\frac{\omega^{(2)}_{ts}}{2}\left(\frac{\kappa^{(2)}_{ts}}{\omega^{(2)}_{ts}}-\phi^2_{ts}\right)^2} p\left(\omega^{(2)}\right) d\omega^{(2)}$$
$$\cdot \frac{e^{\frac{1}{2\sigma^2_{e_{0,s}}}(\phi_{ts}-X^2_{ts}-a_s\vec{\gamma_s})^2}}{\sqrt{2\pi\sigma^2_{e_{0,s}}}} \frac{e^{\frac{1}{2\sigma^2_{a_{0,s}}}(a_s-\mu_{a_{0,s}})^2}}{\sqrt{2\pi\sigma^2_{a_{0,s}}}} \tag{C.8}$$

$$\propto \int_0^\infty e^{-(Z^{(2)}_s-X^{(2)}_s-a_s\vec{\gamma_s}-\vec{e_s})^T\Omega^{(2)}_s(Z^{(2)}_s-X^{(2)}_s-a_s\vec{\gamma_s}-\vec{e_s})/2} p(w^{(2)})d\omega^{(2)} \tag{C.9}$$
$$\cdot\, e^{(\phi_s-X^{(2)}_s-a_s\vec{\gamma_s})^T(\sigma_{e_{0,s}})^{-1}\mathbb{I}(\phi_s-X^{(2)}_s-a_s\vec{\gamma_s})} e^{\frac{1}{2\sigma^2_{a_{0,s}}}(a_s-\mu_{a_{0,s}})^2}\, \mathcal{I}(-1<a_s<1)$$

Hence, the conditional posterior distribution of a_s is,

$$a_s \sim Normal\left(\mu_{a_s}, V_{a_s}\right)\mathcal{I}(-1 < a_s < 1) \quad , \tag{C.10}$$

$$\text{where} \quad V_{a_s} = \left[\vec{\gamma_s}^T \Omega_s^{(2)} \vec{\gamma_s} + \vec{\gamma_s}^T (\sigma^2_{e_{0,s}})^{-1} \mathbb{I}\ \vec{\gamma_s} + (\sigma^2_{a_{0,s}})^{-1}\right]^{-1} \quad , \tag{C.11}$$

$$\text{and} \quad \mu_{a_s} = V_{a_s}\left[\vec{\gamma_s}^T \Omega_s^{(2)}\left(Z_s^{(2)} - X_s^{(2)} - \vec{e_s}\right) + \vec{\gamma_s}^T (\sigma^2_{e_{0,s}})^{-1} \mathbb{I}\left(\phi_s - X_s^{(2)}\right) + (\sigma^2_{a_{0,s}})^{-1}\mu_{a_{0,s}}\right] \tag{C.12}$$

Sampling of $\vec{e_s}$:
Let $\vec{e_s} = \left([e_{ts}]_{t=1}^n\right)^T$. Using the same derivation as above and equation (C.9), we find the distribution of $\vec{e_s}$,

$$p\left(\vec{e_s} \,|\, \cdot\right) \propto \prod_{t=1}^{n} p\left(N_{ts} \,|\, \phi_{ts}\right) p\left(e_{ts}\right) \tag{C.13}$$

$$\propto \int_0^\infty e^{-(Z_s^{(2)} - X_s^{(2)} - a_s\vec{\gamma_s} - \vec{e_s})^T \Omega_s^{(2)} (Z_s^{(2)} - X_s^{(2)} - a_s\vec{\gamma_s} - \vec{e_s})/2}\ p(\omega^{(2)}) d\omega^{(2)} \cdot \frac{e^{\vec{e_s}^T (\sigma^2_{e_{0,s}})^{-1} \mathbb{I} \vec{e_s}}}{\sqrt{2\pi\sigma^2_{e_{0,s}}}} \tag{C.14}$$

Thus, the distribution of $\vec{e_s}$ is,

$$\vec{e_s} \sim Normal\left(\mu_{e_s}, V_{e_s}\right) \quad , \tag{C.15}$$

$$\text{where} \quad V_{e_s} = \left[\Omega_s^{(2)} + (\sigma^2_{e_{0,s}})^{-1}\mathbb{I}\right]^{-1} \tag{C.16}$$

$$\text{and} \quad \mu_{e_s} = V_{e_s}\left[\Omega_s^{(2)}\left(Z_s^{(2)} - X_s^{(2)} - a_s\vec{\gamma_s}\right)\right] \tag{C.17}$$

Sampling of $\vec{\beta_s}$:
To find the conditional posterior distribution of $\vec{\beta_s}$, we look at the likelihood

function

$$p\left(\vec{\beta}_s \,|\, \cdot\right) \propto \prod_{t=1}^{n} p\left(Z_{ts} \,|\, N_{ts}, \psi_{ts}\right) p\left(\psi_{ts} \,|\, \varepsilon_{ts}\right) p\left(\vec{\beta}_s\right) \tag{C.18}$$

$$\propto \prod_{t=1}^{n} \binom{N_{ts}}{Z_{ts}} \left(\frac{e^{\psi_{ts}}}{1+e^{\psi_{ts}}}\right)^{Z_{ts}} \left(\frac{1}{1+e^{\psi_{ts}}}\right)^{N_{ts}-Z_{ts}} \tag{C.19}$$
$$\cdot\, p\left(\psi_{ts} \,|\, \varepsilon_{ts}\right) p\left(\vec{\beta}_s\right)$$

$$\propto \prod_{t=1}^{n} \binom{N_{ts}}{Z_{ts}} \frac{\left(e^{\psi_{ts}}\right)^{Z_{ts}}}{\left(1+e^{\psi_{ts}}\right)^{N_{ts}}} \frac{e^{\frac{-1}{2\sigma^2_{\varepsilon_{0,s}}}(\psi_{ts}-X^{(1)}_{ts}\vec{\beta}_s-\mu_{\varepsilon_{0,s}})^2}}{\sqrt{2\pi\sigma^2_{\varepsilon_{0,s}}}} \tag{C.20}$$
$$\cdot\, e^{-(\vec{\beta}_s-m_{\beta_0})^T P^{-1}_{\beta_0}(\vec{\beta}_s-m_{\beta_0})/2}$$

Applying integral identity (C.3), we can write the likelihood above in terms of ψ_{ts}:

$$p\left(\vec{\beta}_s \,|\, \cdot\right) \propto \prod_{t=1}^{n} 2^{-N_{ts}} e^{\kappa^{(1)}_{ts}\psi_{ts}} \int_0^\infty e^{\omega^{(1)}_{ts}\psi^2_{ts}/2} p\left(\omega^{(1)}\right)\, d\omega^{(1)}$$
$$\cdot\, \frac{e^{\frac{-1}{2\sigma^2_{\varepsilon_{0,s}}}(\psi_{ts}-X^{(1)}_{ts}\vec{\beta}_s-\mu_{\varepsilon_{0,s}})^2}}{\sqrt{2\pi\sigma^2_{\varepsilon_{0,s}}}} e^{-(\vec{\beta}_s-m_{\beta_0})^T P^{-1}_{\beta_0}(\vec{\beta}_s-m_{\beta_0})/2}\,, \tag{C.21}$$

where $\kappa^{(1)}_{ts} = Z_{ts} - N_{ts}/2$. Thus, Theorem 1 implies that the mixing distribution is $\omega^{(2)}_{ts}|\phi_{ts} \sim \mathcal{PG}\left(N_{ts}, \psi_{ts}\right)$.

Let $\vec{\kappa_s}^{(1)} = \left(\left[\kappa_{ts}^{(1)}\right]_{t=1}^{n}\right)^T$, $Z_s^{(1)} = \left(\left[\frac{ks^{(1)}}{\omega_{ts}^{(1)}}\right]_{t=1}^{n}\right)^T$ and $\Omega_s^{(1)} = \text{diag}\left(\omega_{1s}^{(1)}, \cdots, \omega_{ns}^{(1)}\right)$. Then,

$$p\left(\vec{\beta_s} \mid \cdot\right) \propto \int_0^\infty \prod_{t=1}^{n} e^{-\frac{\omega_{ts}^{(1)}}{2}\left(\frac{\kappa_{ts}^{(1)}}{\omega_{ts}^{(1)}} - \psi_{ts}^2\right)^2} p\left(\omega^{(1)}\right) d\omega^{(1)}$$
$$\cdot\, e^{\frac{-1}{2\sigma_{\varepsilon_{0,s}}^2}(\psi_{ts} - X_{ts}^{(1)}\vec{\beta_s} - \mu_{\varepsilon_{0,s}})^2}\; e^{-(\vec{\beta_s} - m_{\beta_0})^T P_{\beta_0}^{-1}(\vec{\beta_s} - m_{\beta_0})/2} \tag{C.22}$$

$$\propto \int_0^\infty e^{-\frac{1}{2}\left(Z_s^{(1)} - X_s^{(1)}\vec{\beta_s} - \vec{\varepsilon_s}\right)^T \Omega_s^{(1)} \left(Z_s^{(1)} - X_s^{(1)}\vec{\beta_s} - \vec{\varepsilon_s}\right)} p\left(\omega^{(1)}\right) d\omega^{(1)} \tag{C.23}$$
$$\cdot\, e^{-\frac{1}{2}\left(\psi_s - X_s^{(1)}\vec{\beta_s} - \mu_{\varepsilon_{0,s}}\right)^T (\sigma_{\varepsilon_{0,s}}^2)^{-1}\mathbb{I}\left(\psi_s - X_s^{(1)}\vec{\beta_s} - \mu_{\varepsilon_{0,s}}\right)}$$
$$\cdot\, e^{-\frac{1}{2}\left(\vec{\beta_s} - m_{\beta_0}\right)^T P_{\beta_0}^{-1}\left(\vec{\beta_s} - m_{\beta_0}\right)}$$

Completing the square yields the following distribution for $\vec{\beta_s}$:

$$\vec{\beta_s} \sim \; Normal\left(\mu_{\vec{\beta_s}}, V_{\vec{\beta_s}}\right) \tag{C.24}$$

$$\text{where} \quad V_{\vec{\beta_s}} = \left[X_s^{(1)}\left(\Omega_s^{(1)} + (\sigma_{\varepsilon_{0,s}}^2)^{-1}\mathbb{I}\right) + P_{\beta_0}^{-1}\right]^{-1} \text{ and} \tag{C.25}$$

$$\mu_{\vec{\beta_s}} = V_{\vec{\beta_s}}\left[X_s^{(1)}\Omega_s^{(1)}\left(Z_s^{(1)} - \vec{\varepsilon_s}\right) + (\sigma_{\varepsilon_{0,s}}^2)^{-1}X_s^{(1)}\left(\psi_s - \mu_{\varepsilon_{0,s}}\right) + P_{\beta_0}^{-1}m_{\beta_0}\right]. \tag{C.26}$$

Sampling of ε_{ts}:
Let $\vec{\varepsilon_s} = \left([\varepsilon_{ts}]_{t=1}^{n}\right)^T$. Using the same decomposition shown in equation (C.23), the joint likelihood for $\vec{\varepsilon_s}$ is

$$p\left(\vec{\varepsilon_s} \mid \cdot\right) \propto \prod_{t=1}^{n} p\left(Z_{ts} \mid N_{ts}, \psi_{ts}\right) p\left(\vec{\varepsilon_s}\right) \tag{C.27}$$

$$\propto \int_0^\infty e^{-\frac{1}{2}\left(Z_s^{(1)} - X_s^{(1)}\vec{\beta_s} - \vec{\varepsilon_s}\right)^T \Omega_s^{(1)} \left(Z_s^{(1)} - X_s^{(1)}\vec{\beta_s} - \vec{\varepsilon_s}\right)} p\left(\omega^{(1)}\right) d\omega^{(1)}$$
$$\cdot\, e^{-\frac{1}{2}\left(\vec{\varepsilon_s} - \mu_{\varepsilon_{0,s}}\right)^T (\sigma_{\varepsilon_{0,s}}^2)^{-1}\mathbb{I}\left(\vec{\varepsilon_s} - \mu_{\varepsilon_{0,s}}\right)}\;. \tag{C.28}$$

Thus, $\vec{\varepsilon_s}$ follows a normal distribution with parameters,

$$\vec{\varepsilon_s} \sim Normal\left(\mu_{\vec{\varepsilon_s}}, V_{\vec{\varepsilon_s}}\right) \tag{C.29}$$

$$\text{where} \quad V_{\vec{\varepsilon_s}} = \left[\Omega_s^{(1)} + \left(\sigma^2_{\varepsilon_{0,s}}\right)^{-1} \mathbb{I}\right]^{-1} \tag{C.30}$$

$$\text{and} \quad \mu_{\vec{\varepsilon_s}} = \left[\Omega_s^{(1)} \left(Z_s^{(1)} - X_s^{(1)}\, \vec{\beta_s}\right) + \left(\sigma^2_{\varepsilon_{0,s}}\right)^{-1} \mu_{\varepsilon_{0,s}}\right]. \tag{C.31}$$

Sampling of λ_{ts}:

To sample λ_{ts}, we use the negative binomial distribution of N_{ts},

$$p\left(\lambda_{ts} \,|\, \cdot\right) \propto p\left(N_{ts} \,|\, \lambda_{ts}\right) p\left(\lambda_{ts}\right) \tag{C.32}$$

$$\propto \frac{\left(\lambda_{ts}\right)^{N_{ts}} e^{-\lambda_{ts}}}{N_{ts}!} \cdot \frac{1}{\Gamma(h)\left(\frac{p_{ts}}{1-p_{ts}}\right)^h} \left(\lambda_{ts}\right)^{h-1} e^{-\lambda_{ts}/\left(\frac{p_{ts}}{1-p_{ts}}\right)} \tag{C.33}$$

$$\propto \left(\lambda_{ts}\right)^{N_{ts}+h-1} e^{-\lambda_{ts}\left(1+\frac{p_{ts}}{1-p_{ts}}\right)} \tag{C.34}$$

$$\propto \left(\lambda_{ts}\right)^{N_{ts}+h-1} e^{-\lambda_{ts}\left(1+\frac{1}{p_{ts}}-1\right)} \tag{C.35}$$

$$\propto \left(\lambda_{ts}\right)^{N_{ts}+h-1} e^{-\frac{\lambda_{ts}}{p_{ts}}} \tag{C.36}$$

Hence, λ_{ts} follows a Gamma distribution with shape parameter $N_{ts} + h$ and scale parameter p_{ts}, i.e.,

$$\lambda_{ts} \sim \mathcal{G}amma\left(N_{ts} + h, p_{ts}\right) \tag{C.37}$$

Sampling of N_{ts}:

Given that $Z_{ts} \,|\, N_{ts} \sim Binomial\left(N_{ts}, \pi_{ts}\right)$ and $N_{ts} \sim Poisson\left(\lambda_{ts}\right)$, we have that the marginal distribution of Z_{ts} follows a Poisson distribution with rate parameter $\pi_{ts}\lambda_{ts}$,

$$Z_{ts} \sim Poisson\left(\pi_{ts}\lambda_{ts}\right) \tag{C.38}$$

By Bayes rules, we have that

$$N_{ts} - Z_{ts} \sim Poisson\left(\left(1 - \pi_{ts}\right)\lambda_{ts}\right) \tag{C.39}$$

Appendix D. Parameter Estimations

Table D.2: Estimated $\vec{\beta_s}$ coefficients with their 90% Confidence Interval for all locations.

Facility	Coef	Mean	Median	90% Conf. Int	
				lower	upper
A	β_1	-1·98301	-2·87585	-4·4810	1·2757
	β_2	-0·0020204	0·003236	-1·6456	1·6315
B	β_1	-1·30041	-1·92976	-3·1829	1·3736
	β_2	0·11357	0·12165	-1·5264	1·7255
C	β_1	-0·80471	-1·23861	-2·0319	1·2903
	β_2	0·014857	0·021477	-1·6388	1·6537
D	β_1	-2·06116	-2·82419	-4·7767	1·3085
	β_2	0·026494	0·027866	-1·5996	1·6605
E	β_1	-1·10048	-1·67059	-2·6604	1·3374
	β_2	0·048162	0·037346	-1·6061	1·7042
F	β_1	-0·94115	-1·41497	-2·5246	1·4503
	β_2	0·16089	0·16539	-1·4811	1·7988
G	β_1	-0·71879	-1·05832	-2·0139	1·3215
	β_2	0·039300	0·036963	-1·5996	1·6957
H	β_1	-0·98055	-1·49157	-2·3781	1·3095
	β_2	0·0084821	0·016313	-1·6058	1·6455
I	β_1	-0·70491	-1·09014	-1·8739	1·3001
	β_2	0·022349	0·021148	-1·6176	1·6657
J	β_1	-0·96685	-1·45703	-2·4120	1·3141

Table D.2: Estimated $\vec{\beta_s}$ coefficients with their 90% Confidence Interval for all locations.

Facility	Coef	Mean	Median	90% Conf. Int	
				lower	upper
	β_2	0·036615	0·040357	-1·6142	1·6813
K	β_1	-0·83426	-1·28090	-2·1207	1·3438
	β_2	0·055580	0·046813	-1·5663	1·6813
L	β_1	1·26970	1·59546	-1·3200	3·4638
	β_2	-0·005757	-0·013282	-1·6650	1·6647
M	β_1	-0·18888	-0·30551	-1·3055	1·3144
	β_2	0·050945	0·056434	-1·5930	1·6640
N	β_1	0·32784	0·37297	-1·1410	1·5896
	β_2	0·13592	0·13555	-1·4972	1·7790

Table D.3: Estimated ratios for a_s by location along with the 90% confidence interval.

Facility	Mean	Median	90% Conf. Int	
			lower	upper
A	0·064371	0·062732	-0·104865	0·235365
B	0·075738	0·075819	-0·091659	0·239276
C	0·119560	0·118169	-0·024537	0·271463
D	0·058017	0·057467	-0·105399	0·224653
E	0·249851	0·250210	0·103090	0·395005
F	0·122342	0·122619	-0·034707	0·280635
G	0·318125	0·318466	0·184318	0·449081
H	0·279283	0·278859	0·141133	0·413762
I	0·178254	0·177557	0·025735	0·328457
J	0·303776	0·304538	0·169531	0·435167
K	0·306361	0·306897	0·187298	0·424489
L	0·334436	0·333574	0·216690	0·454484
M	0·274937	0·275520	0·137353	0·411050
N	0·416922	0·416648	0·299533	0·536780

Appendix E. Summary of SARS-CoV-2 (N1)/PMMoV ratio with alternative probabilities

Table E.4: Selected SARS-CoV-2 (N1) copies per ml normalized by pepper mild mottle virus (PMMoV) copies per ml as a ratio (from observed data) by location which can confirm one case with 50% probability.

Facility	SARS-CoV-2 (N1)/PMMoV			Mean of $p_{ts} \geq 0 \cdot 5$
	Minimum	Median	Mean	
A	$2{\cdot}2550\times10^{-7}$	$3{\cdot}0477\times10^{-4}$	$1{\cdot}4231\times10^{-3}$	0·68720
B	$9{\cdot}4500\times10^{-6}$	$2{\cdot}3350\times10^{-4}$	$2{\cdot}1445\times10^{-3}$	0·70163
C	$1{\cdot}3913\times10^{-6}$	$6{\cdot}2590\times10^{-4}$	$1{\cdot}7391\times10^{-3}$	0·76319
D	$2{\cdot}0650\times10^{-6}$	$1{\cdot}6331\times10^{-3}$	$6{\cdot}2072\times10^{-3}$	0·81814
E	$5{\cdot}1500\times10^{-7}$	$5{\cdot}4854\times10^{-4}$	$6{\cdot}2694\times10^{-3}$	0·77407
F	$2{\cdot}7050\times10^{-6}$	$1{\cdot}1072\times10^{-3}$	$3{\cdot}3144\times10^{-2}$	0·83129
G	$3{\cdot}5300\times10^{-6}$	$8{\cdot}6709\times10^{-4}$	$1{\cdot}6464\times10^{-3}$	0·80803
H	$1{\cdot}3085\times10^{-6}$	$2{\cdot}6386\times10^{-4}$	$1{\cdot}2609\times10^{-3}$	0·77954
I	$8{\cdot}0850\times10^{-7}$	$6{\cdot}2133\times10^{-4}$	$2{\cdot}1970\times10^{-3}$	0·77555
J	$1{\cdot}0900\times10^{-5}$	$6{\cdot}8039\times10^{-4}$	$1{\cdot}2382\times10^{-3}$	0·79152
K	$6{\cdot}9125\times10^{-6}$	$4{\cdot}5700\times10^{-4}$	$1{\cdot}2733\times10^{-3}$	7·22460
L	$4{\cdot}3200\times10^{-7}$	$3{\cdot}5732\times10^{-5}$	$3{\cdot}8508\times10^{-4}$	0·67637
M	$1{\cdot}0333\times10^{-6}$	$4{\cdot}0959\times10^{-4}$	$1{\cdot}9216\times10^{-2}$	0·76447
N	$2{\cdot}0067\times10^{-6}$	$1{\cdot}3448\times10^{-4}$	$6{\cdot}0338\times10^{-4}$	0·75499

Table E.5: Selected SARS-CoV-2 (N1) copies per ml normalized by pepper mild mottle virus (PMMoV) copies per ml as a ratio (from observed data) by location which can confirm one case with 60% probability.

Facility	SARS-CoV-2 (N1)/PMMoV			Mean of $p_{ts} \geq 0 \cdot 6$
	Minimum	Median	Mean	
A	$9{\cdot}1132\times10^{-5}$	$1{\cdot}2819\times10^{-3}$	$2{\cdot}4953\times10^{-3}$	0·83125
B	$9{\cdot}4500\times10^{-6}$	$8{\cdot}0960\times10^{-4}$	$3{\cdot}1131\times10^{-3}$	0·79422
C	$1{\cdot}3913\times10^{-6}$	$9{\cdot}4546\times10^{-4}$	$1{\cdot}9298\times10^{-3}$	0·79432
D	$2{\cdot}4200\times10^{-5}$	$2{\cdot}0288\times10^{-3}$	$6{\cdot}5950\times10^{-3}$	0·83799
E	$3{\cdot}1467\times10^{-5}$	$1{\cdot}3235\times10^{-3}$	$7{\cdot}6061\times10^{-3}$	0·82870
F	$8{\cdot}2350\times10^{-6}$	$2{\cdot}2208\times10^{-3}$	$3{\cdot}9712\times10^{-2}$	0·88866
G	$2{\cdot}1770\times10^{-5}$	$1{\cdot}3178\times10^{-3}$	$2{\cdot}0109\times10^{-3}$	0·88219
H	$3{\cdot}4233\times10^{-5}$	$6{\cdot}3417\times10^{-4}$	$1{\cdot}6238\times10^{-3}$	0·85998
I	$2{\cdot}6100\times10^{-6}$	$7{\cdot}9227\times10^{-4}$	$2{\cdot}7765\times10^{-3}$	0·84794
J	$1{\cdot}7997\times10^{-5}$	$1{\cdot}1496\times10^{-3}$	$1{\cdot}4990\times10^{-3}$	0·85966
K	$6{\cdot}9125\times10^{-6}$	$7{\cdot}3037\times10^{-4}$	$1{\cdot}8167\times10^{-3}$	0·82788
L	$7{\cdot}3000\times10^{-7}$	$1{\cdot}1959\times10^{-4}$	$5{\cdot}5338\times10^{-4}$	0·74610
M	$1{\cdot}9133\times10^{-5}$	$1{\cdot}2004\times10^{-3}$	$2{\cdot}7500\times10^{-2}$	0·85983
N	$2{\cdot}0067\times10^{-6}$	$2{\cdot}4362\times10^{-4}$	$7{\cdot}1254\times10^{-4}$	0·81345

Table E.6: Selected SARS-CoV-2 (N1) copies per ml normalized by pepper mild mottle virus (PMMoV) copies per ml as a ratio (from observed data) by location which can confirm one case with 70% probability.

Facility	SARS-CoV-2 (N1)/PMMoV			Mean of $p_{ts} \geq 0 \cdot 7$
	Minimum	Median	Mean	
A	$9{\cdot}1132\times10^{-5}$	$1{\cdot}3276\times10^{-3}$	$3{\cdot}3686\times10^{-3}$	0·89787
B	$2{\cdot}0167\times10^{-5}$	$1{\cdot}2344\times10^{-3}$	$4{\cdot}0051\times10^{-3}$	0·84870
C	$9{\cdot}5500\times10^{-6}$	$1{\cdot}4408\times10^{-3}$	$2{\cdot}6581\times10^{-3}$	0·86946
D	$2{\cdot}4200\times10^{-5}$	$3{\cdot}1539\times10^{-3}$	$8{\cdot}0506\times10^{-3}$	0·88882
E	$3{\cdot}1467\times10^{-5}$	$1{\cdot}8723\times10^{-3}$	$1{\cdot}0193\times10^{-2}$	0·90719
F	$8{\cdot}2350\times10^{-6}$	$2{\cdot}8129\times10^{-3}$	$4{\cdot}1786\times10^{-2}$	0·90285
G	$2{\cdot}1770\times10^{-5}$	$1{\cdot}8279\times10^{-3}$	$2{\cdot}2887\times10^{-3}$	0·91644
H	$3{\cdot}4233\times10^{-5}$	$1{\cdot}1208\times10^{-3}$	$1{\cdot}7890\times10^{-3}$	0·88785
I	$6{\cdot}6894\times10^{-6}$	$2{\cdot}0206\times10^{-3}$	$3{\cdot}4656\times10^{-3}$	0·91467
J	$1{\cdot}7997\times10^{-5}$	$1{\cdot}5287\times10^{-3}$	$1{\cdot}8216\times10^{-3}$	0·93688
K	$8{\cdot}4790\times10^{-5}$	$1{\cdot}2989\times10^{-3}$	$2{\cdot}5344\times10^{-3}$	0·92419
L	$5{\cdot}1900\times10^{-6}$	$4{\cdot}8964\times10^{-4}$	$7{\cdot}5647\times10^{-4}$	0·81888
M	$1{\cdot}9133\times10^{-5}$	$2{\cdot}1806\times10^{-3}$	$3{\cdot}2924\times10^{-2}$	0·90468
N	$2{\cdot}0067\times10^{-6}$	$3{\cdot}0900\times10^{-4}$	$8{\cdot}8362\times10^{-4}$	0·86775

Table E.7: Selected SARS-CoV-2 (N1) copies per ml normalized by pepper mild mottle virus (PMMoV) copies per ml as a ratio (from observed data) by location which can confirm one case with 90% probability.

Facility	SARS-CoV-2 (N1)/PMMoV			Mean of $p_{ts} \geq 0 \cdot 9$
	Minimum	Median	Mean	
A	$1{\cdot}3276\times10^{-3}$	$4{\cdot}6797\times10^{-3}$	$5{\cdot}1567\times10^{-3}$	0·98192
B	$6{\cdot}0593\times10^{-5}$	$2{\cdot}7099\times10^{-3}$	$7{\cdot}9721\times10^{-3}$	0·96334
C	$4{\cdot}4191\times10^{-4}$	$4{\cdot}1305\times10^{-3}$	$4{\cdot}6130\times10^{-3}$	0·96026
D	$2{\cdot}4246\times10^{-3}$	$7{\cdot}4374\times10^{-3}$	$1{\cdot}2727\times10^{-2}$	0·98632
E	$1{\cdot}6570\times10^{-4}$	$3{\cdot}8532\times10^{-3}$	$1{\cdot}5032\times10^{-2}$	0·96987
F	$8{\cdot}6723\times10^{-4}$	$7{\cdot}1838\times10^{-3}$	$6{\cdot}5746\times10^{-2}$	0·97470
G	$3{\cdot}4976\times10^{-4}$	$2{\cdot}6793\times10^{-3}$	$2{\cdot}8130\times10^{-3}$	0·96956
H	$8{\cdot}3551\times10^{-5}$	$2{\cdot}3507\times10^{-3}$	$2{\cdot}7863\times10^{-3}$	0·95608
I	$9{\cdot}9748\times10^{-5}$	$3{\cdot}0372\times10^{-3}$	$4{\cdot}8338\times10^{-3}$	0·96822
J	$4{\cdot}7200\times10^{-5}$	$2{\cdot}0477\times10^{-3}$	$2{\cdot}2551\times10^{-3}$	0·97912
K	$1{\cdot}3570\times10^{-4}$	$1{\cdot}4225\times10^{-3}$	$3{\cdot}0316\times10^{-3}$	0·95641
L	$3{\cdot}4938\times10^{-4}$	$7{\cdot}3263\times10^{-4}$	$1{\cdot}3915\times10^{-3}$	0·94086
M	$9{\cdot}0293\times10^{-5}$	$4{\cdot}3314\times10^{-3}$	$4{\cdot}8042\times10^{-2}$	0·96245
N	$1{\cdot}1576\times10^{-4}$	$7{\cdot}7051\times10^{-4}$	$1{\cdot}3805\times10^{-3}$	0·95013

Table E.8: Selected SARS-CoV-2 (N1) copies per ml normalized by pepper mild mottle virus (PMMoV) copies per ml as a ratio (from observed data) by location which can confirm one case with 95% probability.

Facility	SARS-CoV-2 (N1)/PMMoV			Mean of $p_{ts} \geq 0 \cdot 95$
	Minimum	Median	Mean	
A	$1{\cdot}3276\times10^{-3}$	$4{\cdot}6797\times10^{-3}$	$5{\cdot}1567\times10^{-3}$	0·98192
B	$1{\cdot}2344\times10^{-3}$	$6{\cdot}3462\times10^{-3}$	$1{\cdot}0755\times10^{-2}$	0·97889
C	$1{\cdot}4408\times10^{-3}$	$4{\cdot}6549\times10^{-3}$	$5{\cdot}5934\times10^{-3}$	0·98170
D	$2{\cdot}4246\times10^{-3}$	$7{\cdot}4374\times10^{-3}$	$1{\cdot}2727\times10^{-2}$	0·98632
E	$3{\cdot}3796\times10^{-4}$	$4{\cdot}5999\times10^{-3}$	$1{\cdot}9319\times10^{-2}$	0·98202
F	$1{\cdot}6287\times10^{-3}$	$8{\cdot}9371\times10^{-3}$	$8{\cdot}7049\times10^{-2}$	0·99228
G	$3{\cdot}4976\times10^{-4}$	$2{\cdot}8302\times10^{-3}$	$2{\cdot}8328\times10^{-3}$	0·97475
H	$8{\cdot}3551\times10^{-5}$	$3{\cdot}0363\times10^{-3}$	$3{\cdot}5807\times10^{-3}$	0·97362
I	$1{\cdot}1784\times10^{-3}$	$3{\cdot}2910\times10^{-3}$	$6{\cdot}2833\times10^{-3}$	0·98828
J	$4{\cdot}7200\times10^{-5}$	$2{\cdot}0477\times10^{-3}$	$2{\cdot}2551\times10^{-3}$	0·97912
K	$1{\cdot}3570\times10^{-4}$	$1{\cdot}4225\times10^{-3}$	$3{\cdot}4036\times10^{-3}$	0·97406
L	$7{\cdot}2997\times10^{-4}$	$1{\cdot}3379\times10^{-3}$	$1{\cdot}8779\times10^{-3}$	0·96496
M	$8{\cdot}9398\times10^{-4}$	$4{\cdot}8779\times10^{-3}$	$6{\cdot}7554\times10^{-2}$	0·98123
N	$6{\cdot}0025\times10^{-4}$	$1{\cdot}2014\times10^{-3}$	$1{\cdot}9938\times10^{-3}$	0·97232

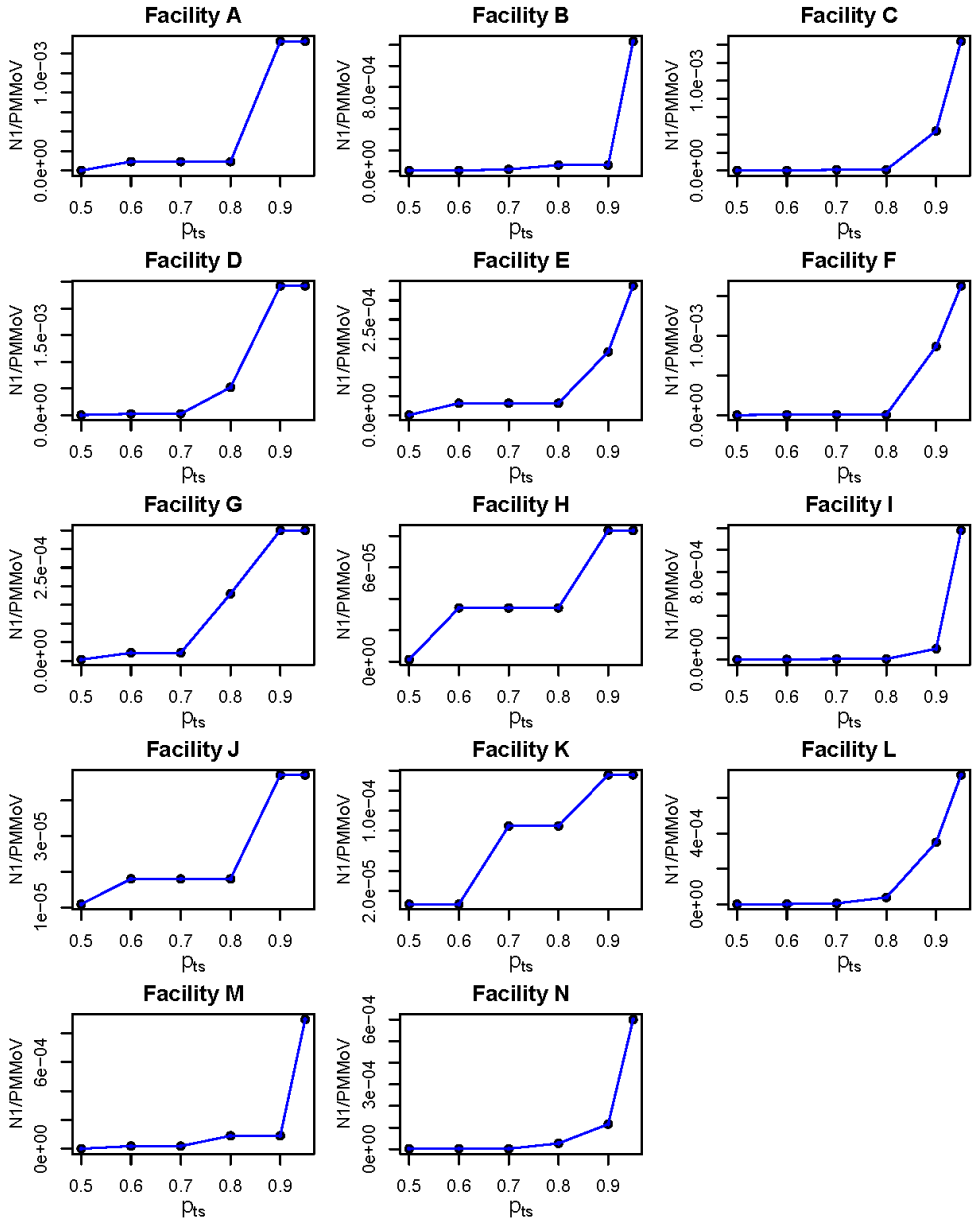

Figure E.4: The minimum value of SARS-CoV-2 (N1) copies per ml normalized by pepper mild mottle virus (PMMoV) copies per ml as a ratio associated with at least one case for different thresholds of reporting probabilities (p_{ts}) at each facility.

Appendix F. Prediction Result

Table F.9: Summary of prediction results for Facility G, H, I during Feb 27th-March 12th, 2022.

Facility	Week (week number)	Observed Z_{ts}	SARS-CoV-2 (N1) / PMMoV	95% C.I of p_{ts}		Predicted mean of p_{ts}
				$2 \cdot 5\%$	$97 \cdot 5\%$	
G	02/27/2022 - 03/05/2022 (57)	22	$6 \cdot 31 \times 10^{-4}$	0·863	0·903	0·884
	03/06/2022 - 03/12/2022 (58)	0	$2 \cdot 19 \times 10^{-5}$	0·600	0·696	0·649
H	02/27/2022 - 03/05/2022 (57)	2	$3 \cdot 57 \times 10^{-5}$	0·714	0·787	0·752
	03/06/2022 - 03/12/2022 (58)	0	$2 \cdot 45 \times 10^{-5}$	0·546	0·645	0·596
I	02/27/2022 - 03/05/2022 (57)	1	$6 \cdot 47 \times 10^{-6}$	0·523	0·618	0·571
	03/06/2022 - 03/12/2022 (58)	1	$2 \cdot 61 \times 10^{-6}$	0·461	0·560	0·511

Table F.10: Summary of prediction results for Facility C, H, L during Feb 5th-15th, 2023.

Facility	Week (week number)	Observed Z_{ts}	SARS-CoV-2 (N1) / PMMoV	95% C.I of p_{ts}		Predicted mean of p_{ts}
				$2 \cdot 5\%$	$97 \cdot 5\%$	
C	02/05/2023 - 02/11/2023 (106)	5	$1 \cdot 13 \times 10^{-3}$	0·711	0·784	0·75
	02/12/2023 - 02/18/2023 (107)	14	$4 \cdot 65 \times 10^{-3}$	0·989	0·992	0·99
	02/19/2023 - 02/15/2023 (108)	3	$9 \cdot 05 \times 10^{-4}$	0·670	0·750	0·71
H	02/05/2023 - 02/11/2023 (106)	9	$2 \cdot 35 \times 10^{-3}$	0·907	0·935	0·92
	02/12/2023 - 02/18/2023 (107)	1	$1 \cdot 40 \times 10^{-3}$	0·775	0·838	0·81
	02/19/2023 - 02/15/2023 (108)	0	$1 \cdot 36 \times 10^{-4}$	0·485	0·587	0·54
L	02/05/2023 - 02/11/2023 (106)	0	$3 \cdot 67 \times 10^{-3}$	0·979	0·986	0·98
	02/12/2023 - 02/18/2023 (107)	0	$1 \cdot 32 \times 10^{-3}$	0·776	0·841	0·81
	02/19/2023 - 02/15/2023 (108)	30	$4 \cdot 38 \times 10^{-4}$	0·569	0·668	0·62

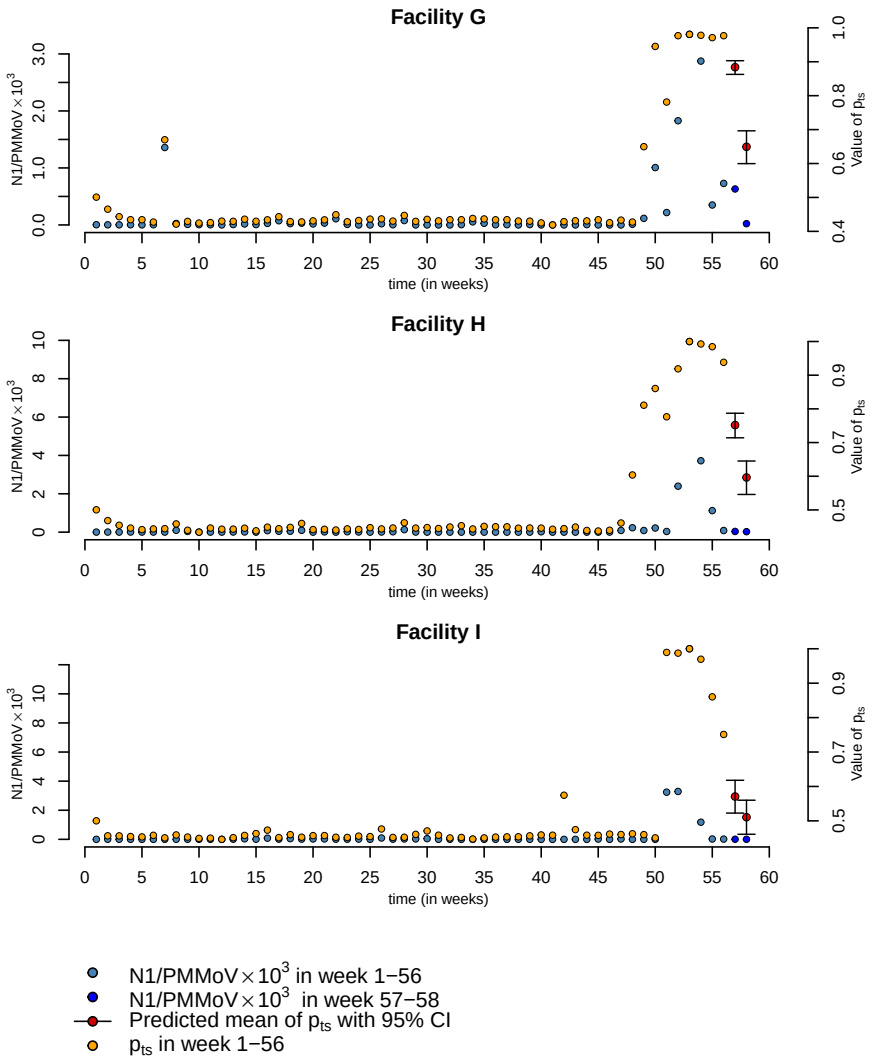

Figure F.5: The figure illustrates the predicted probabilities p_{ts} for weeks 57-58 (highlighted in red circles) by utilizing the SARS-CoV-2 (N1) copies per ml normalized by pepper mild mottle virus (PMMoV) copies per ml as a ratio from weeks 57-58 (green circles) without prior knowledge of the reported positive cases, along with the mean estimated p_{ts} from the training dataset for weeks 1-56 (yellow circles).

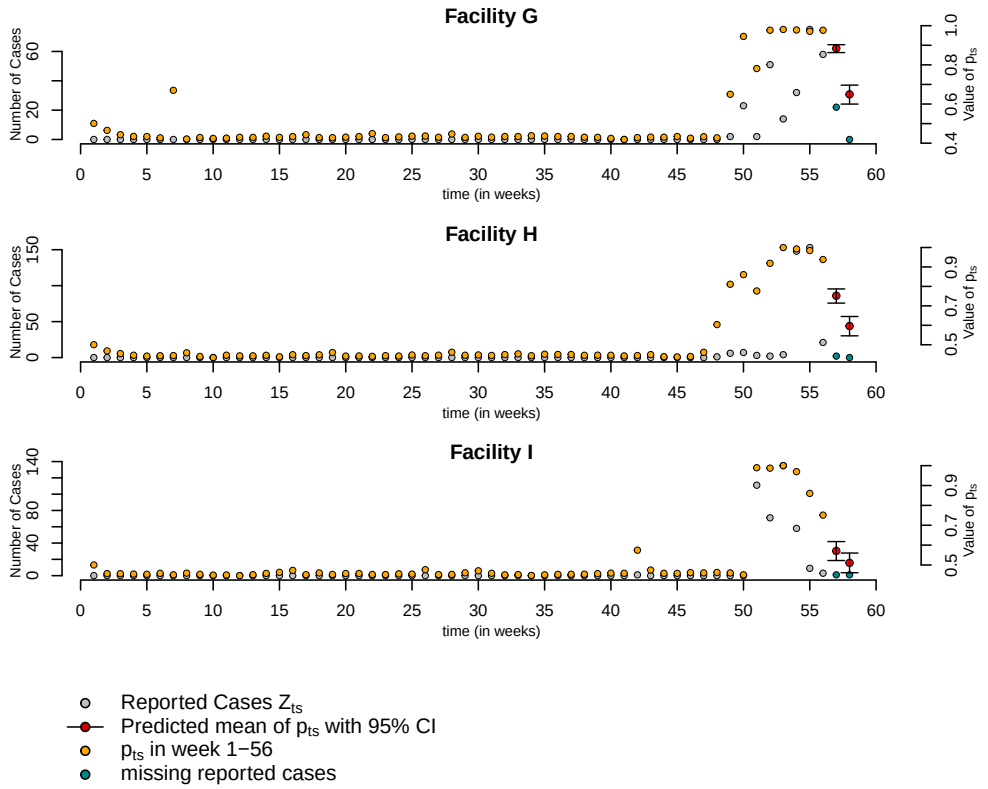

Figure F.6: The figure illustrates the predicted probabilities p_{ts} for weeks 57-58 (highlighted in red circles) by utilizing the SARS-CoV-2 (N1) copies per ml normalized by pepper mild mottle virus (PMMoV) copies per ml as a ratio from weeks 57-58 (green circles) without prior knowledge of the reported positive cases, along with the reported Z_{ts} from the training dataset in weeks 1-56 (grey circles) and in prediction dataset in week 57-58 (green circles).

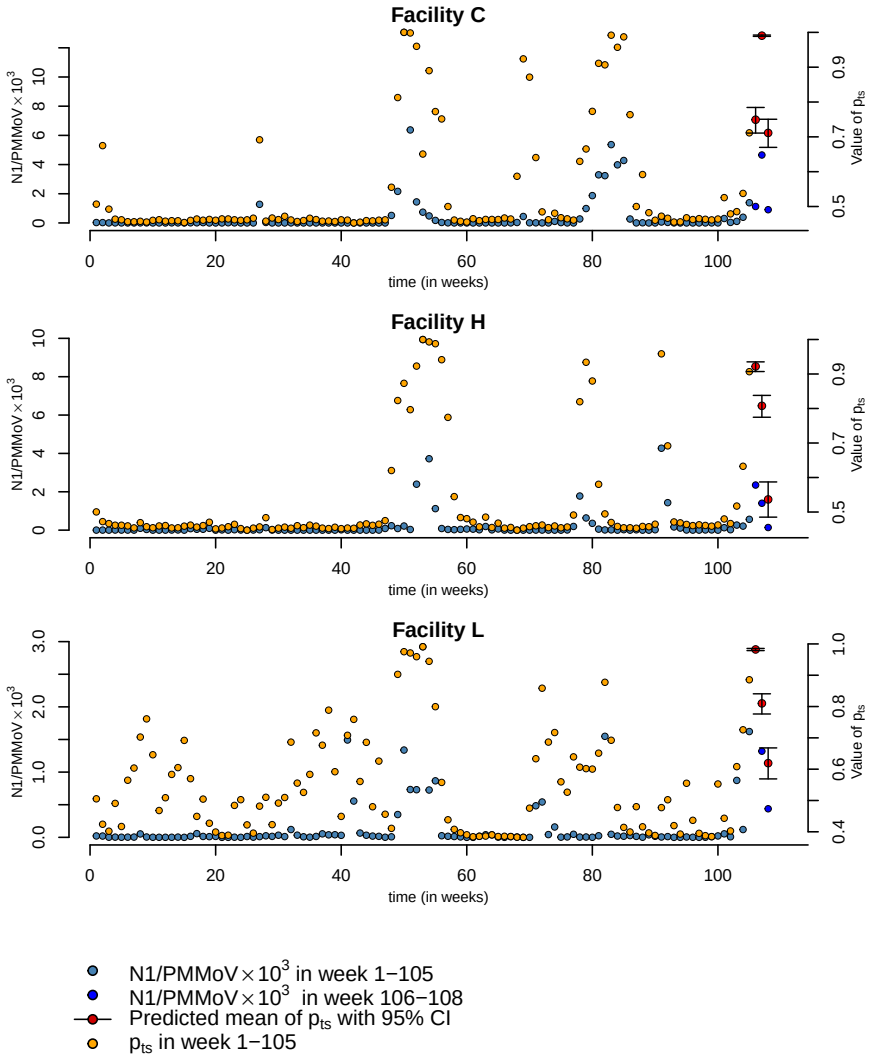

Figure F.7: The figure illustrates the predicted probabilities p_{ts} for weeks 106-108 (highlighted in red circles) by utilizing the SARS-CoV-2 (N1) copies per ml normalized by pepper mild mottle virus (PMMoV) copies per ml as a ratio from week 106-108 (green circles) without prior knowledge of the reported positive cases, along with the mean estimated p_{ts} from the training dataset in weeks 1-105 (yellow circles).

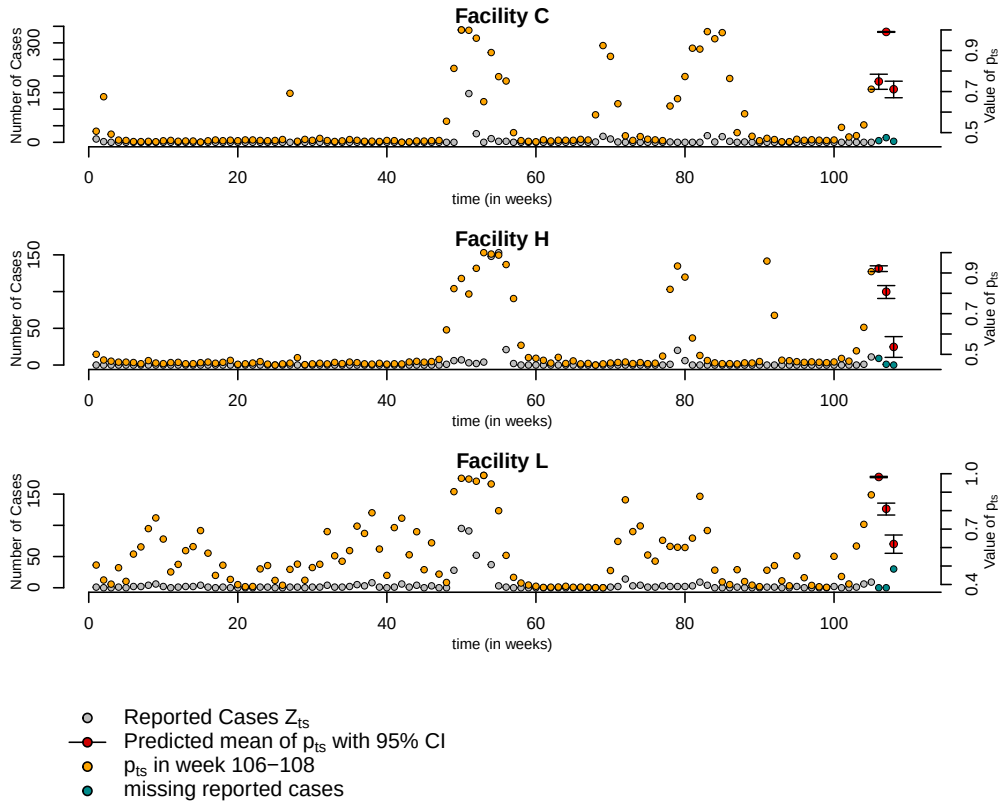

Figure F.8: The figure illustrates the predicted probabilities p_{ts} for weeks 106-108 (highlighted in red circles) by utilizing the SARS-CoV-2 (N1) copies per ml normalized by pepper mild mottle virus (PMMoV) copies per ml as a ratio from weeks 106-108 (green circles) without prior knowledge of the reported positive cases, along with the reported Z_{ts} from the training dataset in weeks 1-105 (grey circles) and in prediction dataset in week 106-108 (green circles).

Appendix G. Sensitivity Analysis

All model parameters have specified prior distributions. This analysis focuses on the two most critical model parameters: the variance of the prior for a_s that impacts the true arrival intensity of true positive cases: $\sigma^2_{a_{0,s}}$, and the covariance matrix of the prior for $\vec{\beta_s}$ that impacts the reporting probability: P_{β_0}. In this sensitivity analysis, we explore different prior specifications to investigate how various priors, which may influence the final thresholds of

SARS-CoV-2 (N1)/PMMoV ratio.

Typically, prior informativeness falls into three categories: informative, weakly informative, and diffuse. Informative priors contain a substantial amount of information about a specific parameter, leading to a high probability mass concentrated within a relatively narrow range of possible values. Weakly informative priors allow for more variation or spread compared to informative priors. On the other hand, diffuse priors offer minimal to no information about the parameter value.

For this study, we assign informative priors $N(0, 0 \cdot 1)$, weakly informative priors $N(0, 1)$, and diffuse priors $N(0, 1000)$ to a_s and $\vec{\beta}_s$, respectively. This results in nine different conditions of priors that we analyze to understand their impact on the thresholds of SARS-CoV-2 (N1)/PMMoV ratio:

(1) $\sigma^2_{a_{0,s}} = 0 \cdot 1 \quad , \quad P_{\beta_0} = 0 \cdot 1\, \mathbb{I}_2$
(2) $\sigma^2_{a_{0,s}} = 0 \cdot 1 \quad , \quad P_{\beta_0} = \mathbb{I}_2$
(3) $\sigma^2_{a_{0,s}} = 0 \cdot 1 \quad , \quad P_{\beta_0} = 1000\, \mathbb{I}_2$
(4) $\sigma^2_{a_{0,s}} = 1 \quad , \quad P_{\beta_0} = 0 \cdot 1\, \mathbb{I}_2$
(5) $\sigma^2_{a_{0,s}} = 1 \quad , \quad P_{\beta_0} = \mathbb{I}_2$
(6) $\sigma^2_{a_{0,s}} = 1 \quad , \quad P_{\beta_0} = 1000\, \mathbb{I}_2$
(7) $\sigma^2_{a_{0,s}} = 1000 \, , \quad P_{\beta_0} = 0 \cdot 1\, \mathbb{I}_2$
(8) $\sigma^2_{a_{0,s}} = 1000 \, , \quad P_{\beta_0} = \mathbb{I}_2$
(9) $\sigma^2_{a_{0,s}} = 1000 \, , \quad P_{\beta_0} = 1000\, \mathbb{I}_2$

where $\sigma^2_{a_{0,s}}$ is the variance of a_s, P_{β_0} is the variance of the vector $\vec{\beta}_s$, and $\mathbb{I}_2$ is the 2×2 identity matrix.

We determine the SARS-CoV-2 (N1)/PMMoV ratio corresponding to $p_{ts} \geq 0 \cdot 8$ and compute the associated summary statistics, including the minimum, median, and mean. The summarized results are presented in the following table, with the respective condition numbers written in the parentheses:

Table G.11: Sensitivity Analysis Table

Facility	SARS-CoV-2 (N1)/PMMoV (combination)		
	Minimum	Median	Mean
A	$9 \cdot 1100 \times 10^{-5}$ (1,2,3,5,6,8,9)	$3 \cdot 0037 \times 10^{-3}$ (1,2,3,5,6,8,9)	$3 \cdot 8903 \times 10^{-3}$ (1,2,3,5,6,8,9)
	$1 \cdot 3276 \times 10^{-3}$ (4,7)	$4 \cdot 6797 \times 10^{-3}$ (4,7)	$5 \cdot 1567 \times 10^{-3}$ (4,7)
B	$6 \cdot 0600 \times 10^{-5}$ (1 - 9)	$2 \cdot 3396 \times 10^{-3}$ (1,2,4,7)	$7 \cdot 0251 \times 10^{-3}$ (1,2,4,7)
		$1 \cdot 9692 \times 10^{-3}$ (3,5,6,8,9)	$6 \cdot 3162 \times 10^{-3}$ (3,6,9)
			$6 \cdot 3818 \times 10^{-3}$ (5,8)
C	$9 \cdot 5500 \times 10^{-6}$ (1 - 9)	$3 \cdot 2386 \times 10^{-3}$ (1,4,7)	$3 \cdot 3877 \times 10^{-3}$ (1,4,7)
		$2 \cdot 7007 \times 10^{-3}$ (2,3,5,6,8,9)	$3 \cdot 2930 \times 10^{-3}$ (2,3,5,6,8,9)
D	$2 \cdot 4246 \times 10^{-3}$ (1,4,5,7)	$7 \cdot 4374 \times 10^{-3}$ (1,4,5,7)	$1 \cdot 2727 \times 10^{-2}$ (1,4,5,7)
	$5 \cdot 2148 \times 10^{-4}$ (2,3,6,8,9)	$6 \cdot 5108 \times 10^{-3}$ (2,3,6,8,9)	$1 \cdot 1371 \times 10^{-2}$ (2,3,6,8,9)
E	$3 \cdot 1500 \times 10^{-5}$ (1 - 9)	$2 \cdot 2117 \times 10^{-3}$ (1,7)	$1 \cdot 1788 \times 10^{-2}$ (1,7)
		$1 \cdot 9448 \times 10^{-3}$ (2,3,5,6,9)	$1 \cdot 0657 \times 10^{-2}$ (2,3,5,6,9)
		$2 \cdot 0783 \times 10^{-3}$ (4,8)	$1 \cdot 1241 \times 10^{-2}$ (4,8)
F	$8 \cdot 2400 \times 10^{-6}$ (1 - 9)	$4 \cdot 2831 \times 10^{-3}$ (1,2,4,5,7,8)	$4 \cdot 9519 \times 10^{-2}$ (1,2,4,5,7,8)
		$3 \cdot 2922 \times 10^{-3}$ (3,6,9)	$4 \cdot 6656 \times 10^{-2}$ (3,6,9)
G	$1 \cdot 7996 \times 10^{-4}$ (1 - 9)	$2 \cdot 5285 \times 10^{-3}$ (1 - 9)	$2 \cdot 6581 \times 10^{-3}$ (1 - 9)

Table G.11: Sensitivity Analysis Table

Facility	SARS-CoV-2 (N1)/PMMoV (combination)		
	Minimum	Median	Mean
H	$8 \cdot 3600 \times 10^{-5}$ (1,4,7)	$1 \cdot 2616 \times 10^{-3}$ (1,4,7)	$2 \cdot 0650 \times 10^{-3}$ (1,4,7)
	$3 \cdot 4200 \times 10^{-5}$ (2,3,5,6,8,9)	$1 \cdot 1208 \times 10^{-3}$ (2,6,9)	$1 \cdot 9296 \times 10^{-3}$ (2,6,9)
		$8 \cdot 7746 \times 10^{-4}$ (3,5,8)	$1 \cdot 8113 \times 10^{-3}$ (3,5,8)
I	$2 \cdot 2800 \times 10^{-5}$ (1,4,7)	$2 \cdot 2221 \times 10^{-3}$ (1,4,7)	$4 \cdot 0314 \times 10^{-3}$ (1,4,7)
	$6 \cdot 6900 \times 10^{-6}$ (2,3,5,6,8,9)	$2 \cdot 1556 \times 10^{-3}$ (2,3,5,6,8,9)	$3 \cdot 6684 \times 10^{-3}$ (2,3,5,6,8,9)
J	$1 \cdot 800 \times 10^{-5}$ (1 - 9)	$1 \cdot 6031 \times 10^{-3}$ (1 - 9)	$1 \cdot 8550 \times 10^{-3}$ (1 - 9)
K	$8 \cdot 480 \times 10^{-5}$ (1 - 9)	$1 \cdot 2989 \times 10^{-3}$ (1 - 9)	$2 \cdot 5344 \times 10^{-3}$ (1 - 9)
L	$3 \cdot 8200 \times 10^{-5}$ (1,2,4,5,8)	$7 \cdot 3130 \times 10^{-4}$ (1,4)	$1 \cdot 1481 \times 10^{-3}$ (1,4)
		$7 \cdot 3263 \times 10^{-4}$ (2,5,8)	$1 \cdot 1936 \times 10^{-3}$ (2,5,8)
	$3 \cdot 4938 \times 10^{-4}$ (3,6,9)	$7 \cdot 3263 \times 10^{-4}$ (3,6)	$1 \cdot 3285 \times 10^{-3}$ (3,6)
		$7 \cdot 9929 \times 10^{-4}$ (9)	$1 \cdot 2899 \times 10^{-3}$ (9)
	$5 \cdot 1900 \times 10^{-6}$ (7)	$7 \cdot 2997 \times 10^{-4}$ (7)	$1 \cdot 0719 \times 10^{-3}$ (7)
M	$9 \cdot 0300 \times 10^{-5}$ (1 - 9)	$3 \cdot 4089 \times 10^{-3}$ (1,2,3,4,6,7)	$3 \cdot 9120 \times 10^{-2}$ (1,2,3,4,6,7)
		$2 \cdot 8076 \times 10^{-3}$ (5,8)	$3 \cdot 7362 \times 10^{-2}$ (5,8)
		$2 \cdot 2064 \times 10^{-3}$ (9)	$3 \cdot 5772 \times 10^{-2}$ (9)
N	$2 \cdot 6800 \times 10^{-5}$ (1 - 9)	$5 \cdot 6938 \times 10^{-4}$ (1 - 9)	$1 \cdot 1400 \times 10^{-3}$ (1 - 9)

Based on the findings presented in Table (G.11), a sensitivity analysis was conducted to assess the impact of different prior conditions on the results. Out of the 14 facilities examined, the majority (9 out of 14) consistently showed similar outcomes concerning the minimum SARS-CoV-2 (N1)/PMMoV ratio corresponding to at least one positive case with a probability greater than 80%. This suggests a degree of robustness in the results across these facilities.

In addition to the consistent findings regarding the minimum SARS-CoV-2 (N1)/PMMoV ratio corresponding to at least one positive case with a probability greater than 80% for the majority of facilities, the sensitivity analysis also revealed potential variations in the median of SARS-CoV-2 (N1)/PMMoV ratio under different prior conditions, especially in conditions 1, 4, and 7, where the covariance matrix P_{β_0} is highly informative. This variability in the median statistic may be attributed to the significant fluctuations in heterogeneous SARS-CoV-2 (N1)/PMMoV ratios observed in these conditions. This observation highlights the sensitivity of the median statistic to the choice of prior. It was noted that imposing hard constraints may limit the ability to express sufficient uncertainty about the available information regarding the reporting probability. Consequently, it is crucial to interpret the results in light of these constraints and their potential influence on the overall conclusions.

However, despite the variations in median values, a notable finding is that the mean of SARS-CoV-2 (N1)/PMMoV ratio corresponding to at least one positive case with a probability greater than 80% remains consistent and close to each other across these nine different prior conditions. This suggests that the mean can serve as a more stable and reliable measure to focus on when comparing the outcomes under various prior conditions.

In conclusion, the sensitivity analysis highlights the importance of considering different prior conditions and their impact on the results. It emphasizes the need for cautious interpretation, especially when dealing with highly informative priors and hard constraints, and underscores the usefulness of the mean as a robust measure for assessing SARS-CoV-2 (N1)/PMMoV ratios corresponding to positive cases with a probability greater than 80% under these different prior scenarios.

The choice of an alternative prior specification can impact the convergence of parameters in the model. Therefore, it is essential to assess model convergence, even if the original prior specification showed no convergence issues. In the present study, the convergence speed and required iteration

number vary across locations based on the current data and experiment.

To ensure convergence, users typically determine the length of the burn-in period using statistical diagnostics while considering the model complexity. If convergence is not achieved for a specific model parameter, practitioners can try doubling or increasing the number of iterations to see if a longer chain resolves the issue.

However, if non-convergence persists, it may indicate that the selected prior is not well-suited for the model or likelihood. In the context of a sensitivity analysis, such results could suggest evidence against choosing that particular prior, given the current model and likelihood.

In the case of these nine different prior conditions in our current experiment, we find that for all locations, the covariance matrix for $\vec{\beta_s}$ needs to be either weakly informative or informative to achieve faster convergence.

Appendix H. Algorithm

The complete algorithm for the Hierarchical Spatial-temporal Model with Lags is summarized in Algorithm 1. The prediction algorithm is summarized in Algorithm 2.

Algorithm 1 Hierarchical Spatial-temporal Model with Lags

Required:(1) Set value of $\sigma_{\varepsilon_{0,s}}$, $\sigma_{e_{0,s}}$, $\sigma_{a_{0,1}}$, P_{β_0}, $\mu_{a_{0,s}}$, and $\mu_{\varepsilon_{0,s}}$, as well as provide value of h, the shape parameter of λ_{ts}; (2) Matrix of recorded cases Z_{ts} for all locations s; (3) $X_{ts}^{(1)}$ and $X_{ts}^{(2)}$, the design matrix containing factors which influence the reporting probabilities and true positive cases, respectively.

for each location $s \in \{1, \cdots, J\}$ **do**

1. Generate $\vec{\varepsilon_s} \sim Normal\left(\mu_{\varepsilon_{0,s}}, \sigma_{\varepsilon_{0,s}}\right)$ and $e_{ts} \sim Normal\left(0, \sigma_{e_{0,s}}\right)$
2. Set $\gamma_{ts} = a_s \gamma_{t-1,s} + e_{ts}$
3. Set $\psi_s = X_s^{(1)} \vec{\beta_s} + \vec{\varepsilon_s}$ and generate $\omega_s^{(1)} \sim \mathcal{PG}\left(N_{ts}, \psi_{ts}\right)$
4. Compute V_{β_s} and μ_{β_s} following equations (C.25) and (C.26) and estimate $\vec{\beta_s}$ from $Normal\left(\mu_{\beta_s}, V_{\beta_s}\right)$
5. Compute V_{ε_s} and μ_{ε_s} following equations (C.30, C.31) and update $\vec{\varepsilon_s}$ from $Normal\left(\mu_{\varepsilon_s}, V_{\varepsilon_s}\right)$
6. Calculate the reporting probabilities π_{ts}
7. Set $\phi_{ts} = X_{ts}^{(2)} + \gamma_{ts}$ and draw $\omega_s^{(2)} \sim \mathcal{PG}\left(N_{ts} + h, \phi_{ts}\right)$
8. Compute V_{a_s} and μ_{a_s} following equations (C.11) and (C.12) and estimate a_s from $Normal\left(\mu_{a_s}, V_{a_s}\right)$
9. Compute V_{e_s} and μ_{e_s} following equations (C.16, C.17) and update e_s from $Normal\left(\mu_{e_s}, V_{e_s}\right)$
10. Update γ_{ts} and calculate p_{ts}, the probabilities associated with N_{ts}
11. Sample $\lambda_{ts} \sim \mathcal{G}amma\left(N_{ts} + h, p_{ts}\right)$ and $N_{ts} \sim Poisson\left(\left(1 - \pi_{ts}\right)\lambda_{ts}\right)$

end for

Algorithm 2 Prediction model

Required: (1) The training results obtained from the Hierarchical Spatio-temporal model with lags; (2) New $X_{ts}^{(1)}$, the design matrix containing factors which influence the reporting probabilities; and (3) New $X_{ts}^{(2)}$, the design matrix containing factors which influence the true positive cases.

for each location $s \in \{1, \cdots, J\}$ **do**

1. Compute the estimated coefficients for a_s and $\vec{\beta_s}$ using the results from Algorithm (1).
2. Generate $\vec{\varepsilon_s} \sim Normal\,(0, 0 \cdot 1)$ and $e_{ts} \sim Normal\,(0, 0 \cdot 1)$
3. Calculate reporting probabilities $\pi_{ts} = \frac{e^{\psi_s}}{1+e^{\psi_s}}$, where $\psi_s = X_s^{(1)}\vec{\beta_s} + \vec{\varepsilon_s}$
4. Compute γ_{1s} and γ_{ts} using the fixed coefficients a_s and $\vec{\beta_s}$ as $\gamma_{1s} = a_s\,\gamma_{-1,s} + e_{ts}$ and $\gamma_{ts} = a_s\,\gamma_{t-1,s} + e_{ts}$, where $\gamma_{-1,s}$ is the estimated value of the last time point in the training model
5. Set $\phi_{ts} = X_{ts}^{(2)} + \gamma_{ts}$ and calculate the probabilities $p_{ts} = \frac{e^{\phi_{ts}}}{1+e^{\phi_{ts}}}$
6. Sample $\lambda_{ts} \sim \mathcal{G}amma\left(h, \frac{p_{ts}}{1-p_{ts}}\right)$ and set $\lambda_{1,s} = \max\{\lambda_{-1,s}, \lambda_{1,s}\}$, where $\lambda_{-1,s}$ is the last time point in the training data set. This is done to accurately capture the number of true cases
7. Generate $Z_{ts} \sim Poisson\,(\pi_{ts}\lambda_{ts})$ and sample $N_{ts} \sim NB\left(h, \frac{1-p_{ts}}{1-\pi_{ts}p_{ts}}\right)$

end for

Appendix I. Model Convergence

A crucial aspect in evaluating the efficacy of our model lies in examining the convergence of its coefficients. The convergence behavior of the coefficients β_1, β_2 and a_s is demonstrated in the Appendix, Figure (I.9) and Figure (I.10), which depicts the final 10,000 iterations from a total of 40,000 iterations conducted using the Markov Chain Monte Carlo (MCMC) algorithm. These convergence plots provide evidence that the MCMC algorithm has successfully converged sufficiently fast, indicating stable and reliable estimates for the model coefficients.

Figure I.9: Last 10000 iterations of $\vec{\beta_s}$ by location showing the convergence of the estimated coefficients.

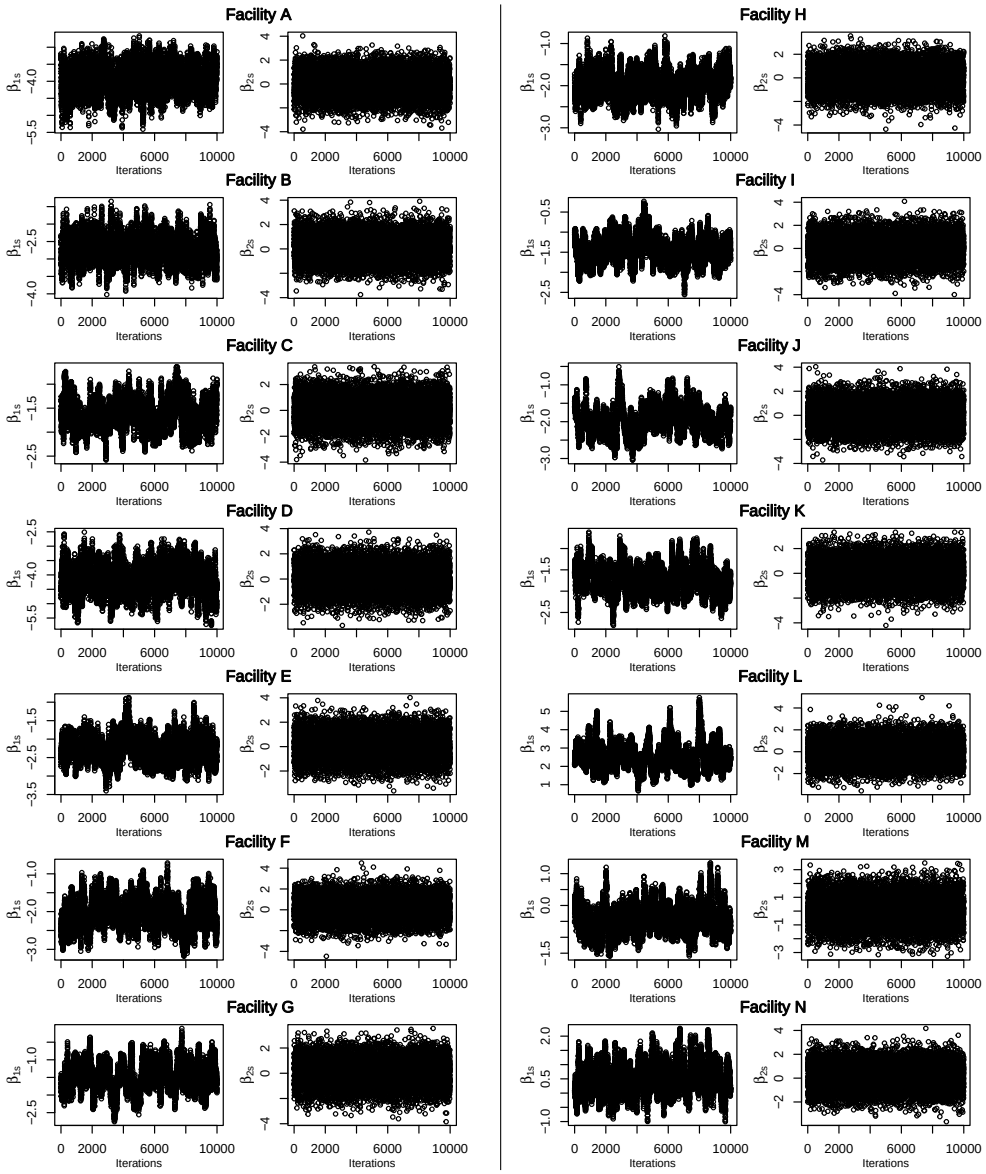

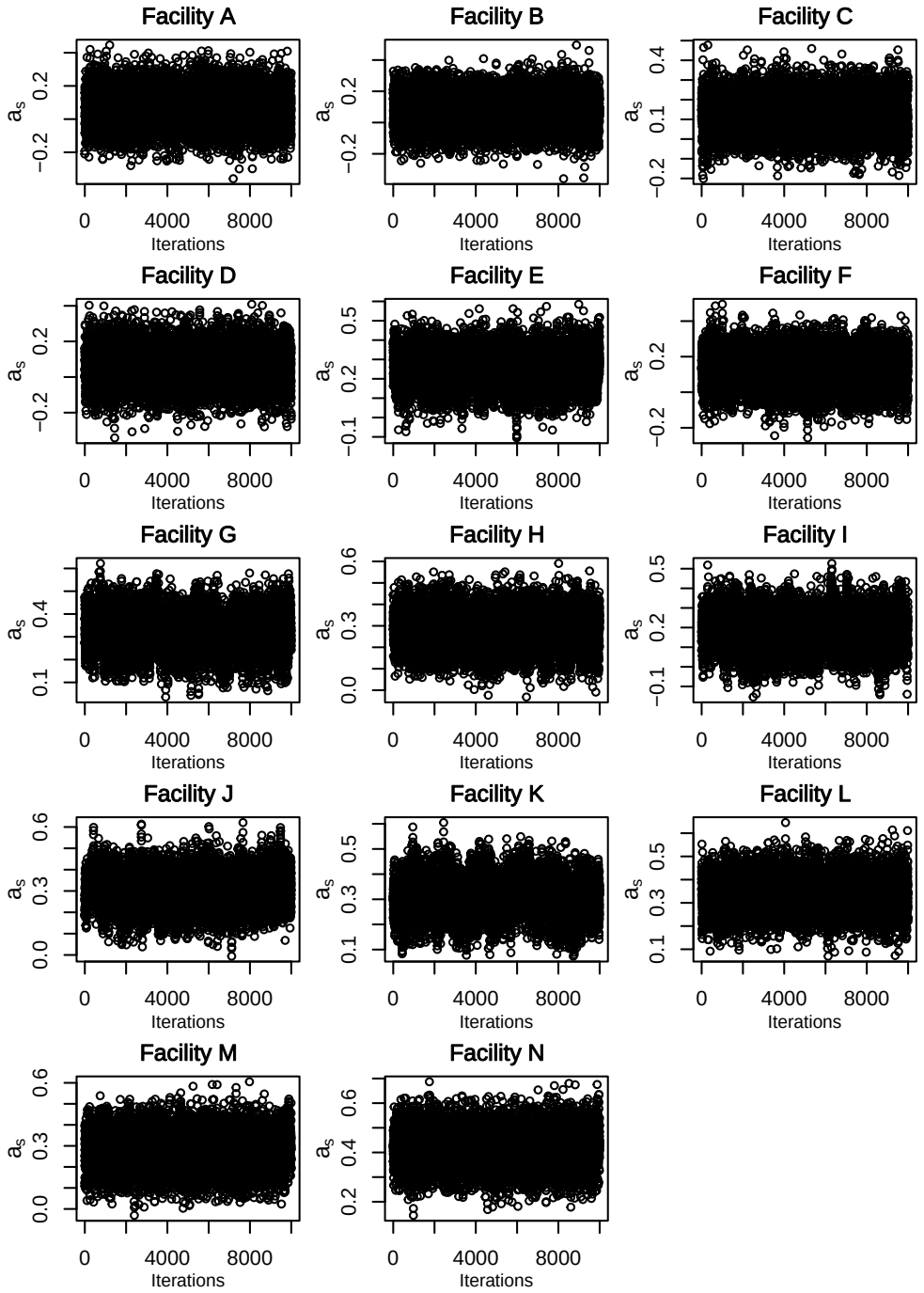

Figure I.10: Last 10000 iterations of a_s by location showing the convergence of the estimated coefficient.

Appendix J. SARS-CoV-2 (N1) Model

The following figures and tables are the results obtained with the unnormalized SARS-CoV-2 (N1) virus concentration.

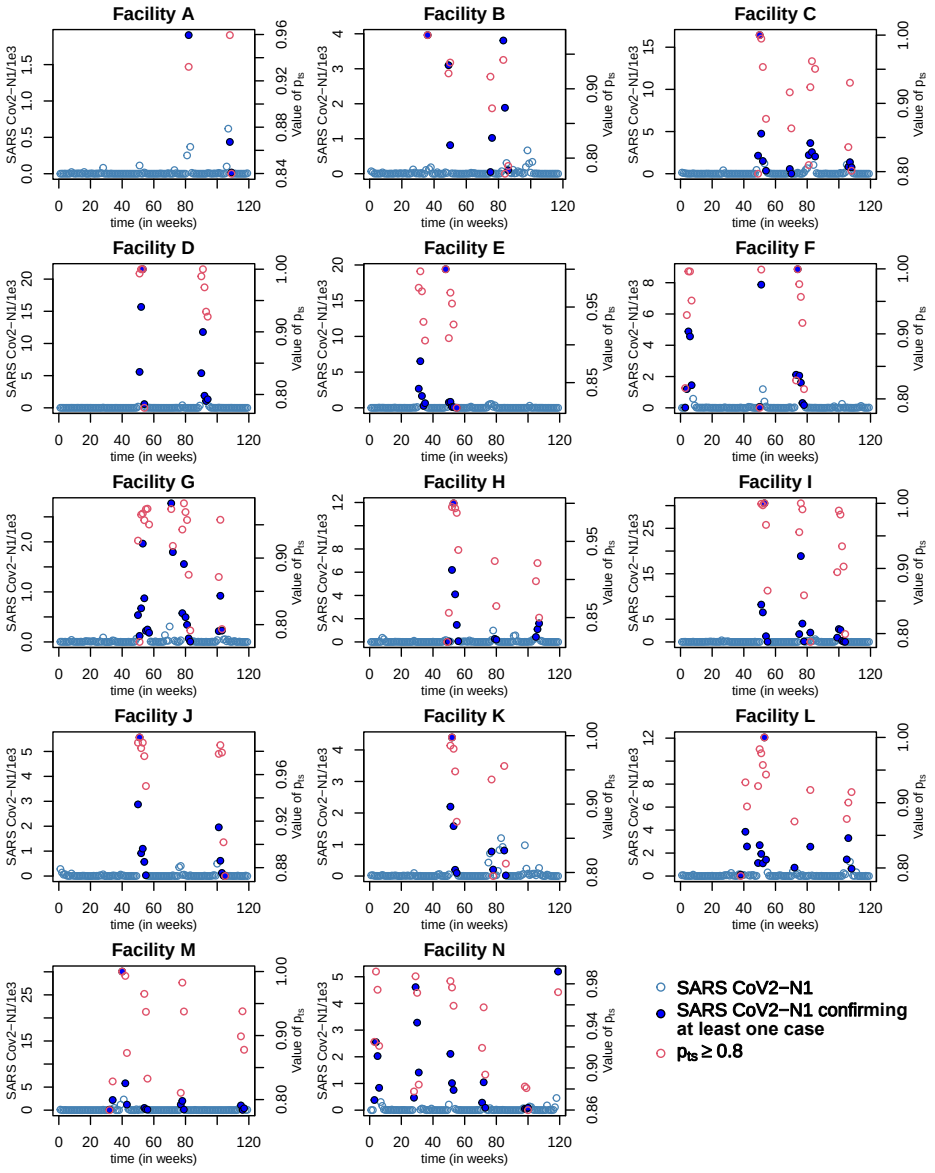

Figure J.11: Value of SARS-CoV-2 (N1) throughout time for all locations, with SARS-CoV-2 (N1) concentration that confirm at least one positive case with 80% probability circled in red. The corresponding $p_{ts} \geq 0 \cdot 8$ is also plotted in red for comparison.

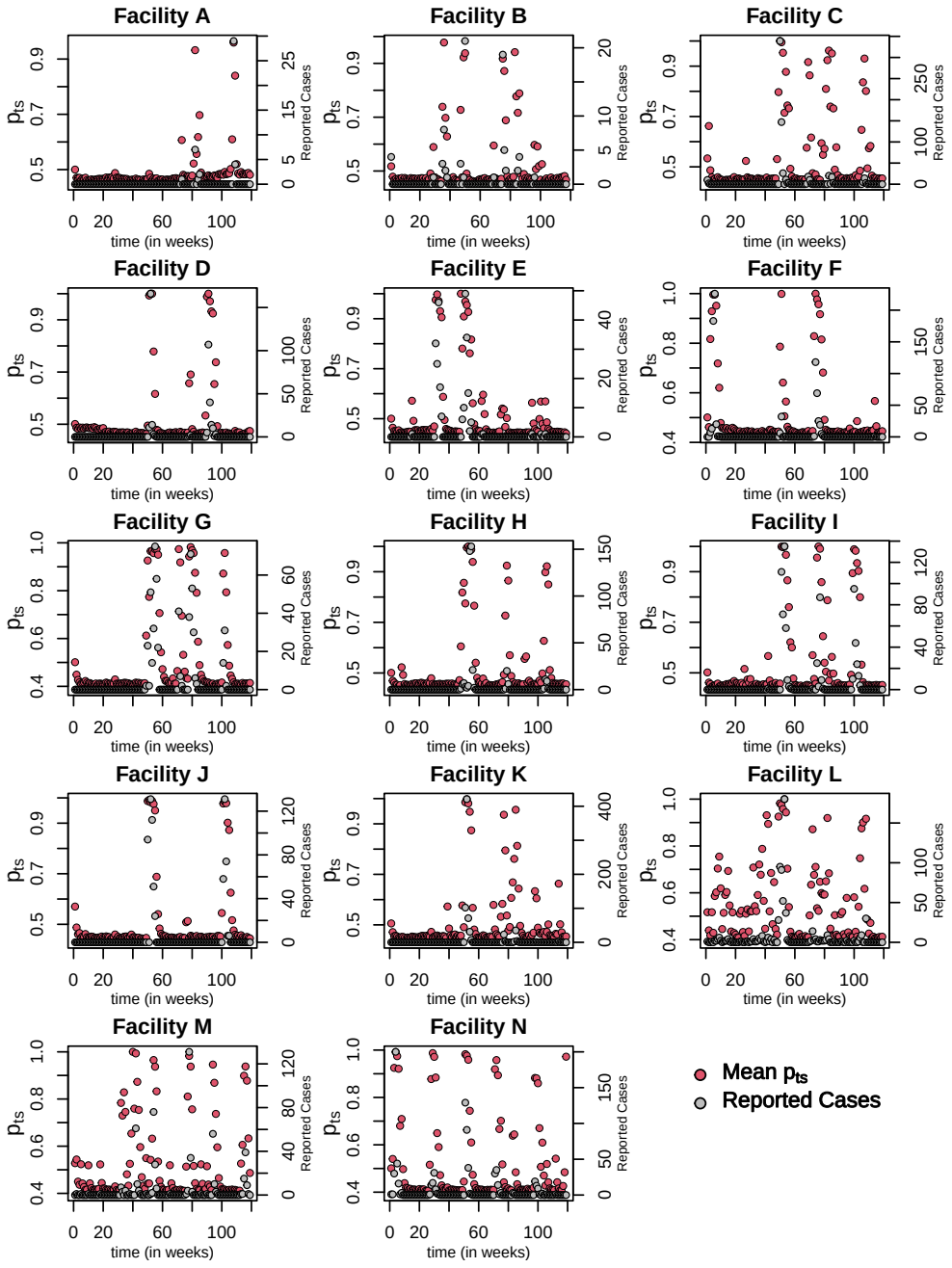

Figure J.12: Estimated p_{ts} probabilities, the probability of at least one positive case versus the number of reported cases, Z_{ts}, by location under the SARS-CoV2-(N1) model.

Table J.12: Estimated SARS-CoV-2 (N1) ratio by location which can confirm one case with 80% probability.

Facility	SARS-CoV-2 (N1)			Mean of $p_{ts} \geq 0 \cdot 8$
	Minimum	Median	Mean	
A	436·896	1171·20	1171·20	0·94510
B	47·895	1454·49	1843·07	0·89269
C	353·786	2045·49	3010·78	0·90346
D	576·888	5380·72	7202·27	0·95318
E	95·763	767·07	3011·25	0·93699
F	64·695	1830·59	2929·55	0·92828
G	69·736	515·55	766·13	0·92861
H	26·580	426·07	2110·06	0·91028
I	44·017	2055·15	5341·16	0·94265
J	29·530	915·04	1526·76	0·98030
K	96·467	793·73	1283·44	0·93313
L	124·707	1686·08	2539·96	0·91896
M	56·818	1018·83	3449·29	0·91485
N	48·763	924·80	1457·87	0·93473

References

1 Nazia N, Butt ZA, Bedard ML, Tang WC, Sehar H, Law J. Methods used in the spatial and spatiotemporal analysis of COVID-19 epidemiology: A systematic review. *Int J Environ Res Public Health* 2022;**19**(14):8267.

2 Kim S, Kim M, Lee S, Lee YJ. Discovering spatiotemporal patterns of COVID-19 pandemic in South Korea. *Sci Rep* 2021;**11**(1):24470.

3 Li G, Denise H, Diggle P, et al. A spatio-temporal framework for modelling wastewater concentration during the COVID-19 pandemic. *Environ Int* 2023;**172**:107765.

4 Giudici P, Tarantino B, Roy A. Bayesian time-varying autoregressive models of COVID-19 epidemics. *Biometrical J* 2023;**65**(1):2200054.

5 Souza APGd, Mota CMdM, Rosa AGF, Figueiredo CJJd, Candeias ALB. A spatial-temporal analysis at the early stages of the COVID-19 pandemic and its determinants: The case of Recife neighborhoods, Brazil. *PloS one* 2022;**17**(5):e0268538.

6 Nikparvar B, Rahman MM, Hatami F, Thill JC. Spatio-temporal prediction of the COVID-19 pandemic in US counties: modeling with a deep LSTM neural network. *Sci Rep* 2021;**11**(1):21715.

7 Winkelmann R. Markov chain Monte Carlo analysis of underreported count data with an application to worker absenteeism. *Empir Econ* 1996;**21**:575-87.

8 Albani V, Loria J, Massad E, Zubelli J. COVID-19 underreporting and its impact on vaccination strategies. *BMC Infect Dis* 2021;**21**:1-13.

9 Stoner O, Economou T, Drummond Marques da Silva G. A hierarchical framework for correcting under-reporting in count data. *J Am Stat Assoc* 2019;**114**(528):1481-92.

10 Polson NG, Scott JG, Windle J. Bayesian inference for logistic models using Pólya–Gamma latent variables. *J Am Stat Assoc* 2013;**108**(504):1339-49.